This is to certify that the

thesis entitled

COMPUTATIONAL ANALYSIS OF PISTON RING WEAR AND
OIL CONSUMPTION FOR AN INTERNAL COMBUSTION ENGINE

presented by

BOON-KEAT CHUI

has been accepted towards fulfillment
of the requirements for

Master degree in Mechanical Engineering

Harold J. Schock
Major professor

Date 6/18/01

COMPUTATIONAL ANALYSIS OF PISTON RING WEAR AND OIL CONSUMPTION FOR AN INTERNAL COMBUSTION ENGINE

By

Boon-Keat Chui

A THESIS

Submitted to
Michigan State University
in partial fulfillment of the requirements
for the degree of

MASTER OF SCIENCE

Department of Mechanical Engineering

2001

ABSTRACT

COMPUTATIONAL ANALYSIS OF PISTON RING WEAR AND OIL CONSUMPTION FOR AN INTERNAL COMBUSTION ENGINE

By

Boon-Keat Chui

Improving the efficiency and reducing the exhaust gas emission have been the goals in the research of internal combustion engines. This thesis presents the fundamental theory in computational modeling of lubrication, piston ring wear and oil consumption in an engine, which play significant roles in influencing the efficiency and emission of the engine. This thesis also presents the predicted results of a study in which the relationship between the piston ring wear and the oil consumption of a 4.6L, V8 engine was analyzed. A computer program, the CASE system (Cylinder kit Analysis System for Engines), together with WEAR and OILCONSUME models were used to simulate the results for this thesis.

The predicted results show that the engine load and speed affected the piston ring wear and the oil consumption significantly. The transient analysis of the piston ring wear show that the piston ring surface experienced high volume loss due to wear during the first 20 hours simulation and reached steady state value after that time period. The transient results of the oil consumption, which consists of oil vaporization and reverse flow through the upper ring gap, did not show significant variation during the 500 hours simulation. However, blow-by into the crankcase showed a significant increase during the 500 hours simulation under the effect of wear.

To my Lord and Savior, Jesus Christ,
to my lovely wife, Gylin,
to my grandmother, my parents and family,
to all my friends.

ACKNOWLEDGEMENTS

I would like to express my appreciation for my advisor, Dr. Harold Schock for his advice, guidance and encouragement toward my progress in completing this thesis. I am also thankful to Jan Chappell, Bobbie Slider, Xiaobing Liu, Stephen Yen, Mahmood Rahi, and all in the engine lab who helped me through the completion of my thesis.

I would like to thank my wife, Gylin for her support, encouragement and prayer. Likewise, thanks to my close friends James and Karen Getz, Rex and Vangie Alocilja for their support and prayer. Without their support and encouragement, it would not have been possible for me to succeed in my Master degree program.

TABLE OF CONTENTS

TABLE OF CONTENTS

TABLE OF CONTENTS

LIST OF TABLES

LIST OF FIGURES

Chapter 1 INTRODUCTION

1.1 Motivation

The world energy shortage has motivated the automotive industry to produce engines that will be more efficient in the future. Petroleum, the main source of energy for today's stereotypical engines will become very limited in a few decades; more energy-saving engines can prolong its usage. Another factor that motivates the engine research is the environmental pollution. Stricter emission regulations have been enforced on automobiles in order to preserve the quality of the environment, because they are considered to be a major contributor to pollution. The automotive industry has been searching for possible solutions. One approach is to design engines that can use alternative energy sources, such as bio-related fuel produced from crops. A second approach would be to invent another type of engine to replace the internal combustion engine, such as a fuel cell powered vehicle; while another approach is to increase the fuel efficiency of engines.

With the two factors mentioned above, it is obvious that the criteria for designing engine should include fulfilling the requirement of high energy efficiency and low pollution level. In other words, engines should have low fuel consumption (high mileage per gallon of fuel) and low emission of toxic gases. Generally, energy efficiency and emission are determined by factors such as the friction level of an engine, the lubrication system and the energy conservation system of an engine.

The main region that contributes to the engine friction and emission is the cylinder kit, which consists of pistons, rings, cylinder bores, connecting rods, bearings as shown in Figure 1.1. The cylinder kit of an engine is considered to be the power source of the engine because it is the region where chemical energy from fuel is transformed into kinetic energy that drives the whole automobile. When the fuel (chemical energy) is ignited in the combustion chamber, the explosive force from the burning fuel pushes the piston into a reciprocating motion (kinetic energy). The highly dynamic forces, during the reciprocating motion in the cylinder kit, often result in the wearing of contact surfaces due to friction. The contacting surfaces include the surfaces between the piston and piston rings, piston and cylinder bore, and piston rings and cylinder bore. In normal operating condition, friction and wear cut scratches in the metal surfaces mentioned above. This causes compression and power loss, and increased oil consumption.

Understanding the physics within the cylinder kit system is crucial for automotive research. It is an important step toward inventing high efficiency engines. However, studying the physics of the engine cylinder kit system is a rather complicated process, because it involves the understanding of heat transfer, fluid mechanics, thermodynamics, and solid mechanics processes that occur during engine operation.

With the advanced computer systems available for complicated calculation, the computational method is becoming a partial approach for engine simulation. Using this method, engineering equations, formulas, and correlations derived from theory and experiments can now be implemented into the computational models, which include analytical and numerical models. The engine cylinder kit system can also be modeled

computationally. In this thesis, computer models of piston ring wear and oil consumption are studied.

1.2 Literature Survey

Michigan State University Engine Research Laboratory(MSUERL) has been putting much effort in the research related to the piston ring wear and the oil consumption. Chung [1] in his Ph.D. dissertation, developed a piston ring wear model through the use of ring dynamics analysis based on several results of experimental efforts in order to study the ring loading effect on the piston ring wear. The simulation results, over the engine speed range between 1200rpm to 2100rpm, showed that higher engine speed operations had lower ring wear rate. Barkman [2] in his M.S. thesis, performed experiment on the measurement of piston ring wear rate of a one-cylinder engine. His results showed that the piston ring wear rate decreased at a relatively high rate to a steady state value after certain hours of operation. Pint [3] developed a mathematical model for the prediction of the tribological system in a simple internal combustion (IC) engine. He designed and developed a software module for the analysis of a three dimensional piston ring wear. His analysis related piston ring twist and piston tilt to the degree of wear in IC engines, under different operating conditions.

For the oil consumption analysis, Ejakov [4] in his Ph.D dissertation, performed ring pack behavior and oil consumption modeling of IC engines. His results showed the importance of modeling ring twist in order to have a more accurate prediction of the piston ring behavior and oil consumption. Qualitative analysis and discussion on oil consumption were performed based on gas dynamic results.

Research in the piston ring wear and the oil consumption was also performed by many researchers from other research institutes. Takashi Inoue et al.[5] performed experimental measurement of transient oil consumption of an automotive engine. Their study showed that the reverse gas flow carries oil from engine crankcase to combustion chamber because of the high vacuum under engine-brake conditions. Min et al.[6] experimentally studied the dynamic characteristics of an oil consumption relationship; between the instantaneous oil consumption and the location of the piston ring gap in IC engines. Their results showed a significant effect of piston rings rotation on oil consumption, under different operation conditions. Tian et al.[7] developed a complete one-dimensional mixed lubrication model to predict oil film thickness and friction of the piston ring-pack. Their study found that the surface roughness has an important impact on oil transport across the piston ring pack into the region above TDC (Top Dead Center). The preliminary comparison showed good agreement between model predictions and the measurements for different engine oils. Wong et al. [8] developed a model to estimate the oil vaporization from the cylinder liner as a contributing mechanism to engine oil consumption. They found that most (74%) of the oil vaporization occurred during intake and compression strokes.

The researchers mentioned above have indeed contributed to a deeper understanding of oil consumption and wear that happen in IC engines. But, discussion and analysis on the relationship between oil consumption and piston ring wear were not performed in depth. Therefore, the objective of this thesis is to extensively study the relationship between the two mechanisms (piston ring wear and oil consumption).

1.3 Problem Statement

Piston ring wear and excessive oil consumption are common problems for an internal combustion engine as the engine gets older. Piston ring wear occurs on the contact surface of the piston rings and cylinder liner, after a certain amount of time of operation. The contact surface experiences high pressure and forces that cause deformation of the geometry and degrading of the quality of the surface material. The distorted surface affects the functionality of the piston rings, and results in energy loss. Because of wear, the piston rings not only lose their sealing power, which prevents gas flow through ring piston ring pack; but also lose their functionality to help in the formation of an oil film layer for lubrication purposes. The excessive oil flow rate through the ring pack and the formation of oil film thickness may be the determining factors for oil consumption. Ejakov's [4] in research on oil consumption and ring pack behavior indicated a close relationship between the ring pack gas flow and oil film thickness, and the oil consumption. There are several mechanisms in oil consumption: oil loss through the vaporization process, and oil flow through piston ring gap during the high pressure gradient between the combustion chamber and piston second land. Other mechanisms such as oil consumption by oil mist and throw-off of liquid droplets, but they are not included in this analysis.

The purpose of this thesis is to implement piston ring model and oil consumption model in the design and analysis of a 4.6L, V8 engine in order to study the relationship between piston ring wear and oil consumption. The design parameters of the 4.6L, V8 engine and its thermodynamic and heat transfer data are used in computer simulations of piston and ring dynamics as well as the prediction of wear and oil consumptions. The

results are to be used to analyze the significance of one mechanism affecting another during engine operation.

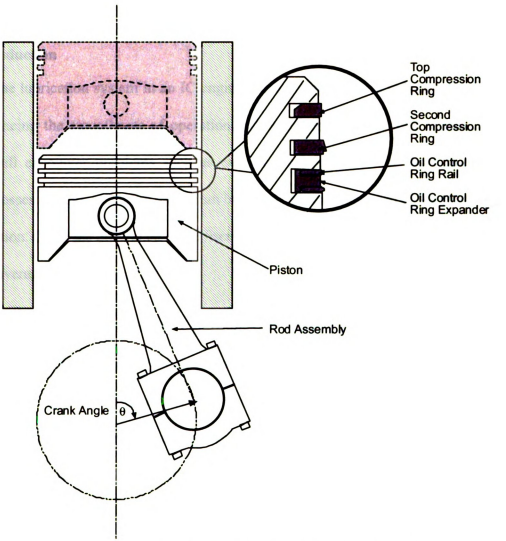

FIGURE 1.1 Cylinder Kit Components of A Basic Engine

Chapter 2 FUNDAMENTALS OF PISTON RING PACK LUBRICATION

2.1 Introduction

The lubrication system in an IC engine plays a major role in reducing the friction and enhancing the smoothness of operation. Without a good lubrication system, an IC engine will encounter problems such as excessive energy loss and short engine life. Friction losses directly affect the maximum brake torque and minimum brake specific fuel consumption. Often the difference in the friction losses distinguishes a good engine design from an average engine design [9].

Figure 2.1 shows the relative significance of different friction work in typical four-cylinder automotive engines (Spark-Ignition, SI) and diesel engines (Compressed-Ignition, CI) at different loads and speeds. The absolute value of the total friction work changes with load, and increases as speed increases. It is observed that friction loss in the cylinder kit (piston-crank) assembly is the major contributor to the total energy loss of engines.

The major design factors that influence cylinder kit assembly friction are the following: ring width, ring face profile, ring tension, ring gap, liner temperature, ring land width and clearances, skirt geometry, and skirt-bore clearance. Usually, cylinder kit assembly friction is dominated by the piston ring friction.

A typical compression ring is separated from the cylinder liner with a thin layer of oil, which acts as the cushion that reduces friction, as shown in Figure 2.2. Depending on the oil film thickness, there are three distinct regions of piston ring lubrication: boundary, mixed, and hydrodynamic as shown in Table 2.1.

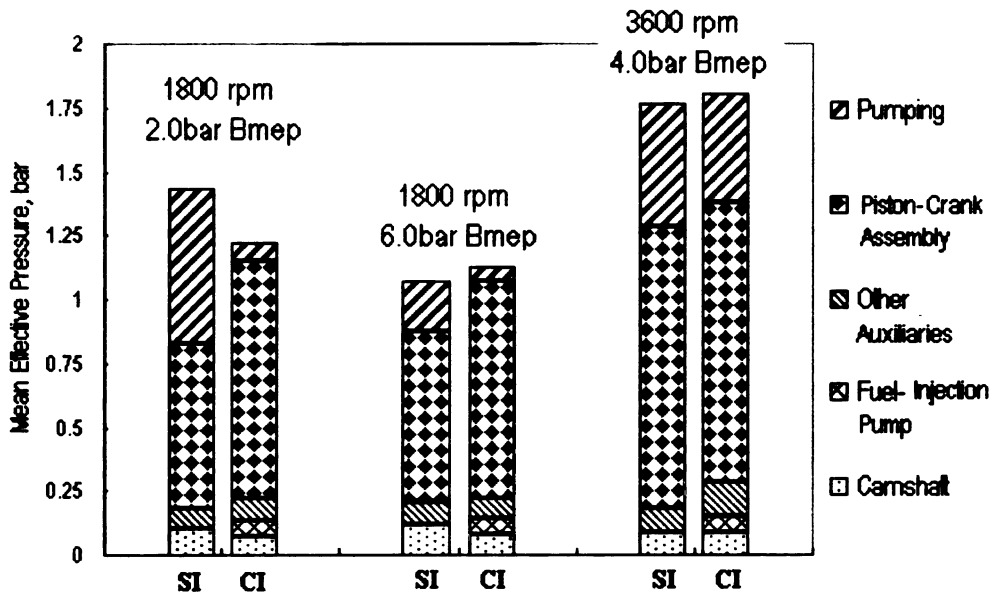

FIGURE 2.1 Comparison of Major Categories of Friction Losses [9]

TABLE 2.1 Regions of Piston Ring Lubrication

Regime of Lubrication	**Lubrication Condition**
Hydrodynamic	Enough oil film between the surfaces, and surface-to-surface contact does not occur
Boundary	Surface-to-surface contact occurs because oil film is not thick enough
Mixed	The intermediate region between hydrodynamic and boundary lubrication

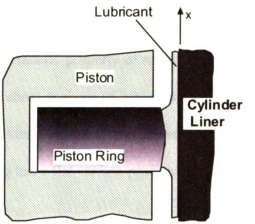

FIGURE 2.2 Compression Ring with Lubricating Oil Film

There are models for the ring and oil film behavior to predict the ring dynamic and oil film formation. The Reynolds equation is used for oil film thickness model of hydrodynamic lubrication. For the practical case where the oil film thickness, h is much less than the ring width, the Navier-Stokes equations for the liquid film motion reduces to a Reynolds equation of the form:

$$\frac{\partial}{\partial x}\left(h^3\frac{\partial p}{\partial x}\right) = -6U\mu\frac{\partial h}{\partial x} + 12\mu\frac{\partial h}{\partial t} \tag{2.1}$$

where:

h	oil film thickness
p	pressure
U	velocity
μ	dynamic viscosity of oil

Oil film thickness is determined by several factors: oil availability to the ring pack, lubricant properties, ring radial tension, gas pressure, ring funning face profiles, engine speed, liner temperature and surface texture.

2.2 Formulating Oil Film Thickness

2.2.1 Oil Viscosity

Viscosity is a characteristic property of oil. Similar to modulus of an elastic solid material, it is used for the shear analysis of lubricants. Oil viscosity affects the formation of oil film thickness. Consider a lubricant film between a cylinder bore and a piston ring. Assume that the piston ring has a flat surface profile, as show in Figure 2.3.

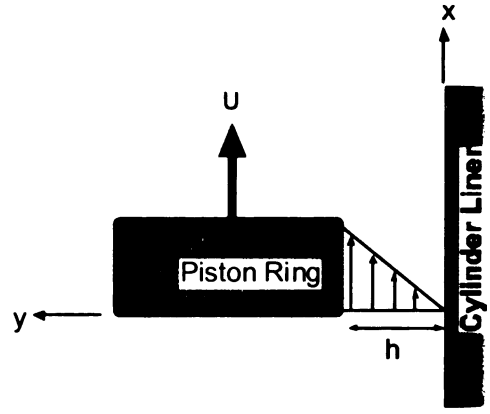

FIGURE 2.3 Linear Velocity Distribution

When the piston ring moves with a velocity U relative to the cylinder bore, a thin layer of oil adheres to the bore such that the velocity of this layer is zero. Another layer of oil simultaneously adheres to the moving ring face and it has the velocity U. The first assumption to be made here is that the oil flows in parallel layers and there are no secondary irregular motions and fluctuations superimposed on the flow; secondly, it is assumed that the flow is laminar. According to the shear stress equation

$$\tau = \frac{F}{A} \tag{2.2}$$

where

τ shear stress

F force required to maintain the flow

A area of the ring face in contact with the oil

If it is assumed linear velocity distribution for the thin oil film, as shown in Figure 2.3, the rate of shearing strain of the oil, γ will become

$$\gamma = \frac{U}{h} \tag{2.3}$$

By definition, the dynamic viscosity of oil is the ratio of shearing stress to the rate of the shearing strain

$$\mu = \frac{shearing\ \ stress}{rate\ \ of\ \ shearing\ \ strain}$$

$$\mu = \frac{F/A}{U/h} = \frac{\tau}{U/h}$$

Thus, the shear stress equation becomes

$$\Longrightarrow \tau = \mu\frac{U}{h} \tag{2.4}$$

For nonlinear velocity distribution as shown in Figure 2.4, the shear stress is

$$\tau = \mu\frac{du}{dy} \tag{2.5}$$

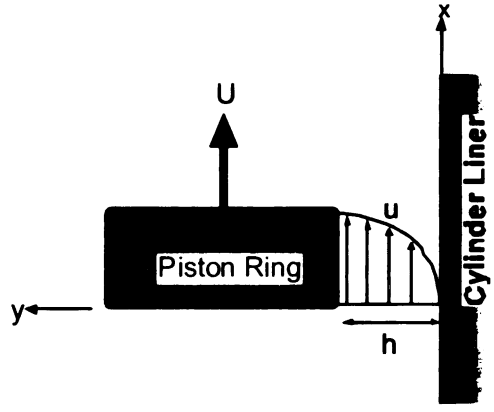

FIGURE 2.4 Nonlinear Velocity Distribution

The SAE (Society of Automotive Engineers) standard engine oil is commonly used by the majority of vehicles today. In the SAE standard, engine oil is separated into different grades according to the viscosity. Viscosity changes with temperature as indicated in Table 2.2.

TABLE 2.2 SAE Oil Viscosity

Oil Grade	Temperature	Viscosity(cP)
SAE 5W	25 ^{0}C	41.45
	100 ^{0}C	4.06
SAE 20W	25 ^{0}C	229.47
	100 ^{0}C	10.50
SAE 50	25 ^{0}C	574.46
	100 ^{0}C	17.99

The relationship between viscosity and temperature for the SAE grades of oil is assumed to follow the Vogel viscosity equation:

$$\mu = ae^{\left(\frac{b}{temperature + c}\right)} \tag{2.6}$$

where *a*, *b*, *c* are Vogel constants

TABLE 2.3 Vogel Constants for SAE Grades Oil

SAE Grade	*a*	*b*	*c*
5W	0.05567	900.0	110.8
20W	0.02370	1361.0	123.3
50	0.01963	1518.0	122.6

2.2.2 Oil Flow in Piston Ring Pack

Oil flow in the piston ring pack needs to be determined for the calculation of oil film thickness. Assume that oil flow in the piston and piston ring pack is similar to a viscous flow through a wide, rectangular slot, as shown in Figure 2.5.

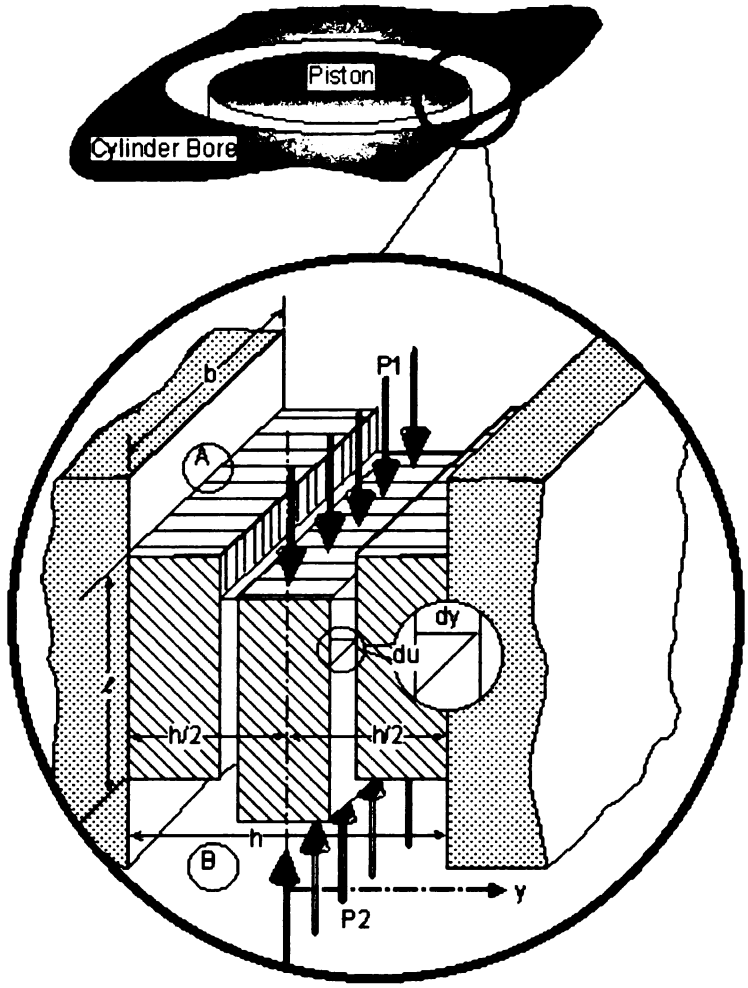

FIGURE 2.5 Oil Flow Through a Rectangular Slot

Consider the slot where the width b is much bigger than the gap h so that we can neglect flow losses at the end; consider also that the length ℓ is much bigger than the gap so that we can neglect losses at the entrance and the exit of the slot. It is a fair assumption

because the clearance between piston and piston rings, and cylinder wall is very small (in the order of 10^{-4} meter) in comparison to the perimeter of cylinder wall, which is about 100 times bigger in magnitude. The downward driving force for the flow is the pressure gradient between point A and point B:

$$\Delta p = P1 - P2$$

Using Newton's Law, the force is

$$F_d = 2\, y\, b\, \Delta p \tag{2.7}$$

If we assume a nonlinear velocity profile, the shear stress, $\tau = \mu^*(du/dy)$.

Thus, the resisting upward force will become

$$F_u = \tau A = 2\, \ell\, b\, \mu(du/dy) \tag{2.8}$$

Applying static equilibrium for the forces F_d and F_u will results in

$$2\, y\, b\, \Delta p = -\left(2\, l\, b\, \mu \frac{du}{dy}\right) \tag{2.9}$$

$$\Longrightarrow -\frac{\Delta p}{l\mu} y dy = du$$

Equation 2.9 has negative sign on the right hand side because of the negative velocity gradient where u decreases as y increases. Applying boundary conditions

$$u = 0 \quad at \quad y = \pm\frac{h}{2}$$

on the integration of Equation 2.9 results in

$$u = \frac{\Delta p}{2\mu\ell}\left[\frac{h^2}{4} - y^2\right] \tag{2.10}$$

The velocity from Equation 2.10 has a parabolic profile in y direction as shown in Figure 2.6. The maximum velocity at $y = 0$, is

$$u_{max} = \frac{\Delta p h^2}{8\mu\ell}$$

The average velocity is

$$u_{ave} = \frac{2}{3}u_{max} = \frac{\Delta p h^2}{12\mu\ell} \tag{2.11}$$

With the velocity available, we can calculate the volume of flow, Q passes through the slot. Multiplying the average velocity with cross-sectional area, we get

$$Q = \frac{\Delta p b h^3}{12\mu\ell} \tag{2.12}$$

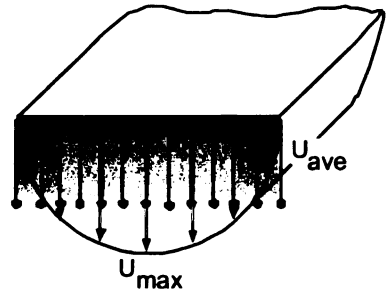

FIGURE 2.6 Parabolic Velocity Distribution

2.2.3 Reynolds Equation for Ring Pack

With the flow rate being determined, we can further derive the oil film thickness formula to obtain the Reynolds equation. The three-dimensional Reynolds equation has the following general form:

$$\frac{\partial}{\partial x}\left(\frac{h^3}{\mu}\frac{\partial p}{\partial x}\right) + \frac{\partial}{\partial z}\left(\frac{h^3}{\mu}\frac{\partial p}{\partial x}\right) = -6U\frac{\partial h}{\partial x} - 6W\frac{\partial h}{\partial z} + 12V \tag{2.13}$$

where

p	oil pressure
μ	oil dynamic viscosity
h	oil film thickness
U	ring axial velocity
W	ring tangential velocity
$V = \frac{dh}{dt}$	ring radial velocity

We can further simplify the Reynolds equation into two-dimensional form if we assume an axisymmetric case of the piston ring lubrication, as shown in Figure 2.7:

$$\frac{\partial}{\partial x}\left(\frac{h^3}{\mu}\frac{\partial p}{\partial x}\right) = -6U\frac{\partial h}{\partial x} + 12\frac{\partial h}{\partial t} \tag{2.14}$$

Equation 2.14 is valid for piston ring lubrication for conditions:

- negligible body forces
- negligible fluid inertia
- constant lubricant pressure throughout the thickness of the oil film
- newtonian fluid for the lubricant

- laminar flow
- no slip at the boundaries

The Reynolds equation will be in the form of Equation 2.1 when constant lubricant viscosity, μ is assumed.

$$\frac{\partial}{\partial x}\left(h^3\frac{\partial p}{\partial x}\right) = -6U\mu\frac{\partial h}{\partial x} + 12\mu\frac{\partial h}{\partial t}$$

Assuming non-deformable surfaces for both the ring and the liner, integrating Equation 2.1 yields

$$p = -6\mu U I_1 + 12\mu\frac{\partial h}{\partial t}I_2 + AI_3 + B \tag{2.15}$$

where:

A, B integration constant

$$I_1 = \int\frac{dx}{h^2}$$

$$I_2 = \int\frac{x}{h^3}dx$$

$$I_3 = \int\frac{dx}{h^3}$$

The integration constants A and B are found from the boundary conditions. Three typical boundary conditions for piston ring lubrication are given in Table 2.4.

TABLE 2.4 Boundary Conditions for Piston Ring Lubrication

Position	Sommerfeld	Half-Sommerfeld	Reynolds
$x = 0$	$p = P1$	$p = P1$	$p = P1$
$x = b/2$	--	$p = 0$	--
$x = b$	$p = P2$	--	$p = P2, \frac{dp}{dx} = 0$

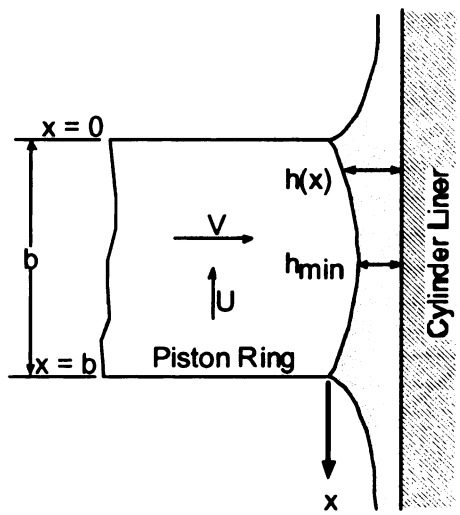

FIGURE 2.7 Piston Ring Lubrication

With defined boundary conditions, and a given piston ring face profile, the hydrodynamic pressure distribution can be determined from Equation 2.15. The hydrodynamic pressure force must be equated by another source of forces. The forces are from the pressure force acting behind the ring and the tension of the ring. The hydrodynamic pressure force acting on the ring face is determined by integrating the pressure, $p(x)$ over the ring face:

$$P = \int_0^b p(x)dx \tag{2.16}$$

For equilibrium in the radial direction as show in Figure 2.8, the pressure force obtained from Equation 2.16 must be equal to the radial ring force, F_R

$$P = F_R \tag{2.17}$$

Then, the minimum oil film thickness (h_{min}) will be determined by satisfying Equation 2.17.

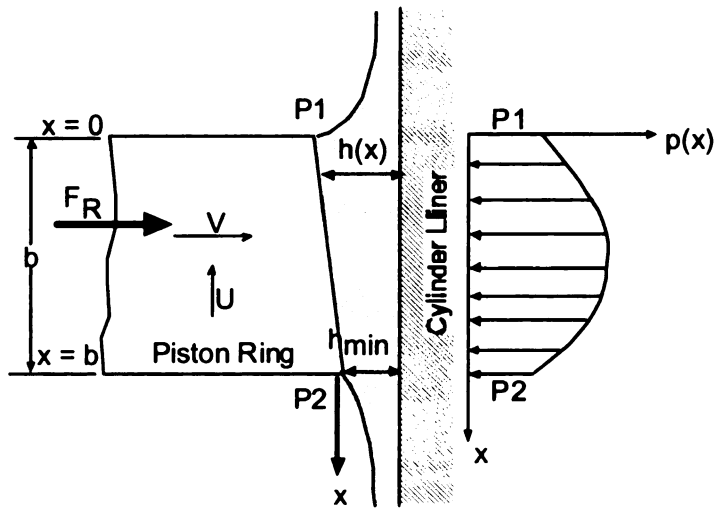

FIGURE 2.8 Forces Acting on a Piston Ring

Chapter 3 FUNDAMENTALS OF PISTON RING WEAR

3.1 Introduction

Cylinder kit components experience extreme mechanical stresses. These mechanical stresses are caused by high kinetic energy and momentum from piston dynamics, high temperature and pressure during combustion, and distortion of metal. A common problem that arising in this environment is wear, as a result of contacts of surface asperities between the rings and the cylinder wall. Therefore, the design of piston ring pack must satisfy the criteria set by durability and efficiency, despite of the severe conditions.

The reciprocating motion of the piston and piston rings against the cylinder liner causes the wearing of the contact surfaces, as shown in Figure 3.1. Recalling that there are three regions of lubrication: boundary, mixed and hydrodynamic, we assume that piston ring wear only occurs in the regime of boundary and mixed lubricant where there is lack of lubricant that avoids surface-to-surface contact.

Generally, wear is caused by the individual and combined effects of corrosion, adhesion, and abrasion. Corrosion occurs when acidic substances within the cylinder kit assembly, such as the products of combustion, attack metal surfaces. Those metal surfaces include the major component of the cylinder kit assembly, such as piston and ring. However, effective prevention has been discovered through the invention of chemical detergent oils that neutralize the corrosive acids and with proper control of the engine

temperature. This type of wear is difficult to model because the issue is more about the problem of chemical reaction. Hence, corrosive wear is assumed negligible in this thesis.

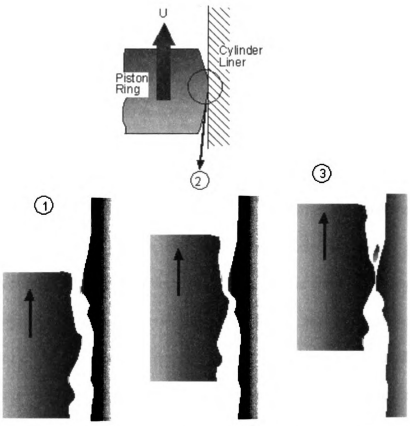

FIGURE 3.1 Rubbing of Two Contact Surface Under Microscopic View

Another type of wear is abrasion. Abrasive wear occurs when there are impurities present in the lubricating oil at the contact surfaces. The impurities can come from atmospheric dust, and from the metallic debris from corrosive and adhesive wear. When the impurities stay between two contact surfaces, such as the piston ring and cylinder liner, the ratio of asperity contact is increased. Abrasion can be eliminated by using air filtration, periodic oil changes and filtration in the oil system. This type of wear will not be included in this thesis.

The third type is adhesive wear. It mainly affects parts of the engine where there is metal-to-metal contact. The cylinder kit assembly experiences this type of wear when there is metal-to-metal contact between the piston, rings, and cylinder walls, and takes place. Adhesive wear is especially significant when the engine is at the beginning of operation and is cold because there is insufficient oil in the cylinder kit assembly. This type of wear is of the focus for this thesis.

3.2 Formulating Piston Ring Adhesive Wear

3.2.1 Surface Texture of Piston Ring

Surface texture affects the wear rate of a surface. Surface texture can be vaguely identified with the roughness and smoothness of a surface. Surface texture representation can be very complex. A complete description of a surface involves many aspects: the amplitude (roughness and smoothness), the waviness (the pattern of surface roughness) and the density of surface asperities per unit surface area. Identifying a surface with only one aspect while neglecting the other will result in inaccurate surface representation.

There are several methods for the representation of the surface texture. A common parameter representing a surface texture is Ten-points-height, R_z. It is the average distance between the five highest peaks and the five deepest valleys of a surface within the sampling length. The formula for R_z is

$$R_z = \frac{(Y_{p1} + Y_{p2} + Y_{p3} + Y_{p4} + Y_{p5}) - (Y_{v1} + Y_{v2} + Y_{v3} + Y_{v4} + Y_{v3})}{5} \qquad (3.1)$$

where:

Y_p's the height of the five highest peaks

Y_v's the depth of the five lowest valleys

Another commonly used parameter is the Roughness Average, R_a. Roughness average is the arithmetic average of the distance of the filtered or unfiltered roughness profile from its mean line, as shown in Figure 3.2.

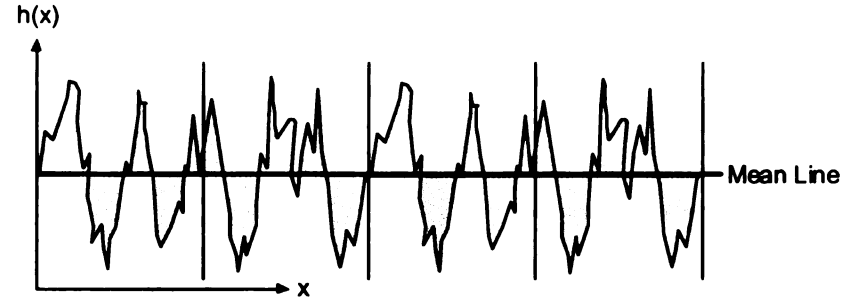

FIGURE 3.2 Surface Profile

The formula for roughness average is as following:

$$R_a = \frac{1}{L}\int_0^L |h(x)|dx \tag{3.2}$$

Another commonly used parameter is the Root Mean Square Roughness Average, R_q. It is the root mean square of the distance of the filtered or unfiltered Roughness profile from its mean line, as shown in Figure 3.2. R_q is the standard deviation of the amplitude density distribution. The amplitude of this parameter is more sensitive to peaks and valleys compared to R_a. The formula for root mean square roughness average is as following:

$$R_q = \sqrt{\frac{1}{L}\int_0^L h^2(x)dx} \tag{3.3}$$

Using R_a and R_q to represent a surface texture is sufficient, except when there are differences in the density of the real contact area. To illustrate this point, we can use two surfaces that have the same value of R_a and R_q, but have different surface texture. Figure 3.3 shows two different surfaces: surface 1 and surface 2.

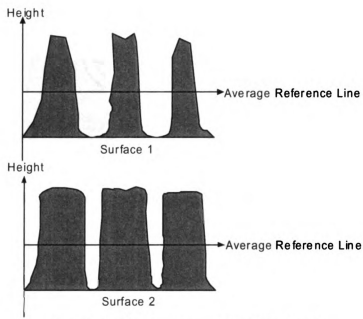

FIGURE 3.3 Engineered Surface Profile

Applying Equation 3.2 and Equation 3.3 will give the same value of R_a and R_q, even though these two surfaces are different. To distinguish surface 1 from surface 2, another parameter is introduced: the Abbott Firestone Curve (*AFC*), which is also called the Bearing Ratio Curve. It is a graphical representation of the bearing ratio parameter, *tp* (length of bearing surface, expressed as a percentage of the assessment length of a surface specimen, at a depth below the highest peak or a selected distance from the average reference line) in relation to the profile level. The curve contains all the amplitude information of a surface profile. The *AFC* for surfaces 1 and 2 is shown in Figure 3.4.

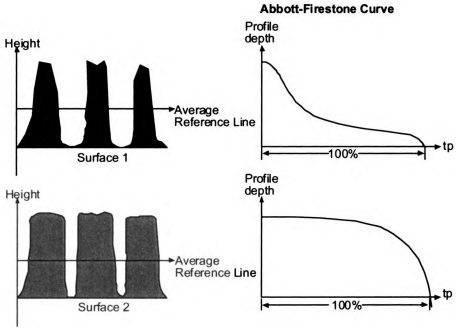

FIGURE 3.4 Surface Representation Using Abbott Firestone Curve

From the Abbott Firestone Curve, one can identify the difference between the two surfaces, where surface 1 has lower amplitude density than surface 2.

In this thesis, we describe the piston ring surface in terms of R_z and the Abbott Firestone Curve. The piston ring surface profile is assumed to be in the shape of cones with the peak angle, β of 45 degrees, as shown in Figure 3.5.

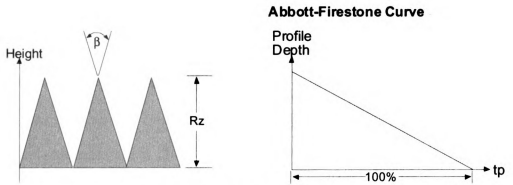

FIGURE 3.5 Piston Ring Surface Profile

The surface of the cylinder liner needs to be modeled too. However, this step can be avoided by assuming that the interaction of two surfaces can be simplified as the interaction of one rough surface with a planar surface. The roughness value will become the combination of the two surfaces roughness.

$$R_z = R_{z1} + R_{z2} \tag{3.4}$$

where

R_z the roughness of the combined surface profile

R_{z1} the roughness of surface one

R_{z2} the roughness of surface two

3.2.2 Wear Mechanism

Consider a small section of piston ring sliding on cylinder bore as shown in Figure 3.6.

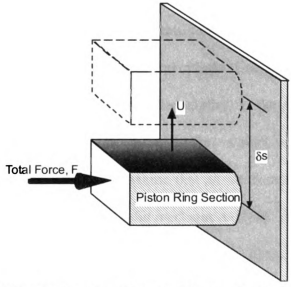

FIGURE 3.6 Piston Ring Sliding on Cylinder Bore

The section of the piston ring is assumed to be very small such that the curvature effect of the piston ring in circumferential direction is negligible. The amount of worn volume from the piston ring surface is calculated using the following equation:

$$\delta V = k \frac{F}{H} \delta s \tag{3.5}$$

where

δV	incremental volume loss from the contact surfaces
δs	sliding distance of one surface with respect to another surface
F	the total load applied to the piston ring surface while it is sliding
H	combined hardness of the piston ring and cylinder liner
k	wear coefficient

Equation 3.5 is only valid when the lubrication is not hydrodynamic. To model this, we can assume that the lubrication is not hydrodynamic when the oil film thickness between the piston ring and the cylinder liner is less than the combined roughness. In the regime of mixed or boundary lubrication, the entire load is assumed to be carried by the metal surface contact between the piston ring and cylinder liner, and the support by the oil film is neglected. To evaluate the total load that applies on the surface, consider that a piston ring pressed against the cylinder bore by forces such as ring tension and the pressure forces behind the piston ring. Assume that all the forces are transferred to the cylinder liner as a normal force. Using a solid mechanic analysis, pressing the ring against the cylinder bore will result in axial force distribution on the piston ring surface, as shown in Figure 3.7.

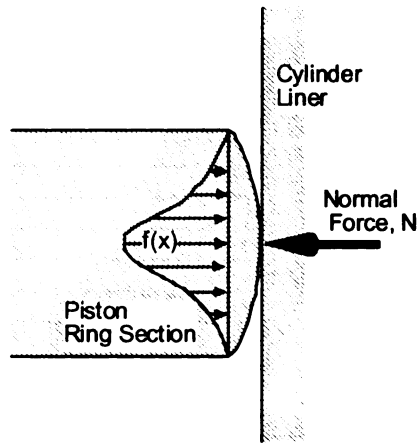

FIGURE 3.7 Ring Section Contact with Cylinder Liner

Applying Newton Second Law, one can deduce that

$$N = F_r \tag{3.6}$$

where

$$F_r = \int f(x)dx \tag{3.7}$$

In order to obtain f(x), the following assumptions are made:

- linear elastic behavior of the piston ring material
- modulus of elasticity of the cylinder liner is infinite
- deformation is very small
- shear stress on the piston ring is negligible compared to normal stress

With the assumptions above, the determination of force distribution begins with the discretization of the piston ring surface into m slices with the same width as shown in Figure 3.8. These slices are assumed to be completely separated from each other since the normal stress is much higher than the shear stress.

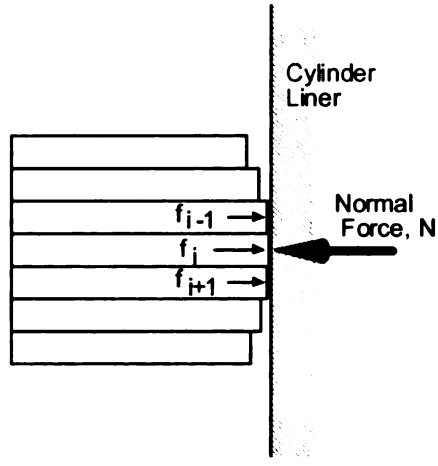

FIGURE 3.8 Discretized Piston Ring Surface

Using Hook's law:

$$\sigma_i = E\ \varepsilon_i \tag{3.8}$$

$$\varepsilon = \frac{\Delta \ell_i}{\ell_i} \tag{3.9}$$

$$f_i = \sigma_i\ A_i \tag{3.10}$$

where:

σ	the normal stress
f	force at each slice
E	the modulus of elasticity of piston ring
ε	the elastic deformation of the piston ring
$\Delta\ell$	the deformation of the length of a slice

ℓ the original length of a slice

A the cross-sectional area of a slice

In order to obtain the force for each slice, an arbitrary reference point is assigned to start the process of evaluating the total force. The process continues with the reference point being varied until the criteria of Equation 3.6 is met. The final value for the force of each slice will be used for the calculation of wear at each slice.

Chapter 4 FUNDAMENTALS OF OIL CONSUMPTION

4.1 Introduction

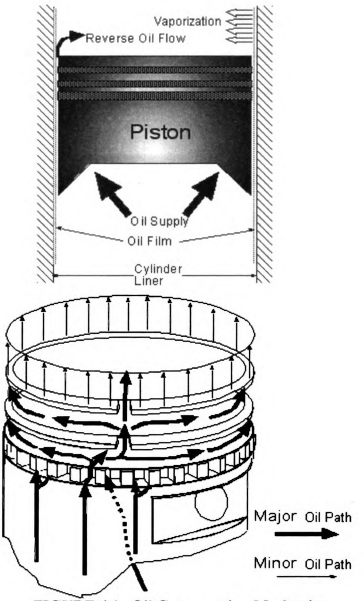

FIGURE 4.1 Oil Consumption Mechanism

Oil consumption is a phenomenon in which the engine oil escapes from the engine crank case into the environment. The engine oil consumption can occur through

various ways: oil leakage through the engine gasket, vaporization of oil from the oil film on the cylinder liner, flow of oil from the engine crank case to the combustion chamber through the piston ring gap, throw-off and blow-by. Oil consumption can be reduced primarily by a better design of the engine crank case sealing system to prevent oil leakage through engine gasket. However, to further reduce oil consumption, one must solve the problems of excessive oil loss through other methods. In this research, two contributors of oil consumption are the main focus: oil vaporization and reverse flow of engine oil through the piston ring endgap as shown in Figure 4.1.

Oil vaporization is associated with the magnitude of the film thickness left on the cylinder bore. The engine oil, which vaporizes from the cylinder liner, diffuses into the cylinder gases and leaves the combustion chamber as either partially burned or unburned hydrocarbon. Hence, reducing the oil vaporization can reduce hydrocarbons in the exhaust gases, and further reduce overall engine emission.

On the other hand, reverse flow of engine oil through the top piston ring endgap is associated with the pressure drop across the piston ring pack. The design of the piston and piston ring, as well as the configuration of piston ring endgaps, influence the oil flow into the combustion chamber.

4.2 Vaporization of Engine Oil from the Cylinder Liner

A vaporization model is used here to predict the amount of oil loss due to heat and mass transfer. It is appropriate to use this model by assuming that the oil film left on the cylinder liner during the intake and exhaust strokes as a liquid surface, while the combustion gas is a gas flow above the surface as shown in Figure 4.2. Because of the

reciprocating motion of the piston ring with respect to the cylinder liner, the area of the cylinder liner exposed to the combustion gases is also changing. The volume of oil vaporized per crank angle, V_{evap} is evaluated using the equation below:

$$V_{evap} = \frac{A\, m'' \Delta t}{\rho_{oil}} \tag{4.1}$$

where:

A area of cylinder bore being exposed to combustion chamber as a function of crank angle

m'' evaporative mass flux

Δt time interval between two successive crank angle

ρ_{oil} engine oil density

The following assumptions must be made in order to use Equation 4.1:

- the rate of oil vaporization is low to be considered a low mass transfer rate convection process
- the change in the engine oil temperature is very small so that its density can be treated as constant
- the temperature of the oil film does not exceed the engine oil boiling point so that the burning of oil does not occur
- the engine oil is considered a single-species fluid for the simplification of the problem

The evaporative mass flux is derived from the mass convection theory where the empirical equations are

$$m''_{evap} = g_m m_f \tag{4.2}$$

$$g_m = \frac{Sh\,\rho_{oil} D_h}{D_c} \tag{4.3}$$

$$m_f = \left(\frac{P_{vapor}}{P_{cylinder}}\right)\left(\frac{MW_{oil}}{MW_{air}}\right) \tag{4.4}$$

$$Sh = a\ Re_D^{\ d}\ Sc^e \tag{4.5}$$

$$Sc = \frac{\nu_{air}}{D_h} \tag{4.6}$$

where:

m''_{evap}	evaporative massflux
g_m	mass transfer coefficient
m_f	mass fraction
Sh	Sherwood number
ρ_{oil}	engine oil density
Dh	binary diffussion coefficient
D_c	hydraulic diameter
P_{vap}	instantaneous vapor pressure of oil
$P_{cylinder}$	instantaneous pressure of combustion gas
MW's	molecular weight
a,d,e	constants

Re_D Reynolds Number

Sc Schmidt Number

ν_{air} air kinematic viscosity

The vapor pressure of different grades of hydrocarbon can be obtained from the *Handbook of Vapor Pressures and Heats of Vaporization of Hydrocarbons and Related Compounds* [11]. The relationship between vapor pressure and surface temperature follow the Antoine equation:

$$\log P_{vap} = A - \frac{B}{C + T_{surface}} \tag{4.7}$$

where

A, B, C Antoine constants for engine oil

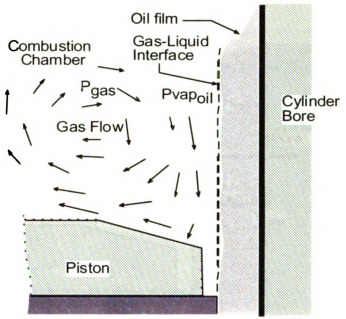

FIGURE 4.2 Vaporization Process at Oil Film

With the Antoine equation, the only unknown variable needed to calculate the vapor pressure is the surface temperature of the oil film. Obtaining the surface temperature of the oil film is possible by using the thermal resistance model. Consider Figure 4.3. With the temperature of the combustion gas and liner known from measurement, we are able to deduce the net heat transfer across the oil film using

$$q_{net} = \frac{T_{liner} - T_{gas}}{R_{total}} \tag{4.8}$$

$$R_{total} = R1 + R2 = \frac{H}{kA} + \frac{1}{hA} \tag{4.9}$$

Since the net heat transfer across the oil film is the same as the heat transfer from T_{liner} to $T_{surface}$, thus

$$q_1 = q_{net} = \frac{T_{liner} - T_{surface}}{R_1} \tag{4.10}$$

$$\Rightarrow T_{surface} = T_{liner} - R_1 q_{net} \tag{4.11}$$

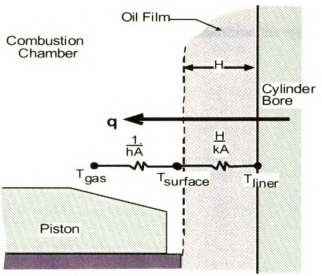

FIGURE 4.3 Thermal Resistance Model for Oil Film

We evaluate the amount of oil loss due to vaporization using Equation 4.1 to Equation 4.11. The results will be added with the amount of oil loss due to another method that will be discussed next.

4.3 Reverse Flow of Engine Oil through Top Compression Ring Gap

Engine oil consumption can be caused by the reverse flow of the oil through the top compression piston ring, when pressure in the second land of the ring pack is higher than the pressure in the combustion chamber. To model this oil loss mechanism, one can apply the theory of laminar viscous flow in a channel or duct. As in Figure 4.4, we assume that the ring gap is a non-circular duct with the length of the ring width, R_w, and it is completely filled with viscous engine oil.

The flow of the engine oil through the ring gap may be a laminar flow or it may be a turbulent flow. Using the dimensionless parameter, Reynolds number, Re- the ratio of the inertia to viscous effects in the flow, we can determine the type of flow through the ring gap. The equation of Reynolds number is

$$Re_D = \frac{\rho u D}{\mu} \tag{4.12}$$

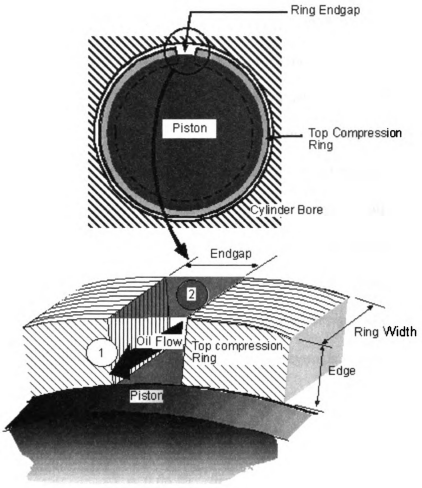

FIGURE 4.4 Flow Through Piston Ring Gap

In the piston ring pack, one can assume the viscous oil flow to be very slow, because the average cross sectional area for oil flow is relatively small (in the order of 10^{-7} meter square) and the viscous effects are dominant. Hence, a low Reynolds number flow is expected and we can categorized the type of flow as laminar for the oil flow through the piston ring end gap.

Another factor that we need to consider is the effect of the entrance region. Including this factor into the calculation of oil flow will be complicated. Therefore, we

need to simplify the problem by assuming a fully developed flow. For this assumption to be valid, the dimension of ring gap and the ring width is important. Consider a pipe system as shown in Figure 4.5. The fluid typically enters the pipe with a nearly uniform velocity profile at section 1. As the fluid moves through the pipe, viscous effects cause it to be retarded by the pipe wall (the non-slip boundary condition.) Due to the boundary layer effects, which are caused by the viscous effects, the velocity profiles change with distance along the pipe. In the region where the velocity profiles are changing, it is called the entrance region. After the entrance region, the velocity profile remains constant and the flow is considered to be fully developed. In the fully developed region, viscous effects are of considerable importance. As with many other properties of pipe flow, the dimensionless entrance length, ℓ_e/D, correlates quite well with the Reynolds number. Typical entrance lengths are given by

$$\frac{\ell_e}{D} = 0.06\,Re \quad for \quad laminar \tag{4.13}$$

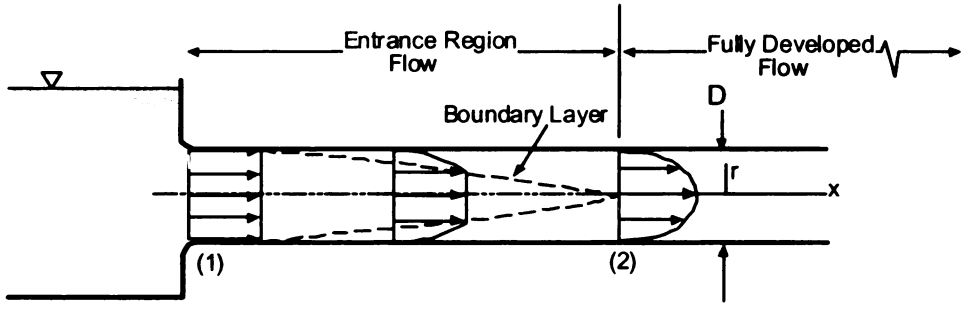

FIGURE 4.5 Different Flow in a Pipe System

To simplify the modeling of the oil flow through the ring gap, we can assume that the effect of the entrance length is negligible, provided that the ratio of the ring width to

the hydraulic diameter of the ring gap channel satisfies Equation 4.13. This assumption is appropriate for a typical IC engine, since the ring gap is relatively small compared to the ring width.

4.3.1 Formulating Reverse Flow Equation

Refer to Figure 4.4, the second land of the piston ring pack is labeled 2, while the combustion chamber is 1. When the pressure at 2 is higher than the presure at 1, the pressure force will push the oil through the ring gap. For simplification in deriving the equation for flow, hydraulic diameter, D will be used for the ring gap cross section and the analysis is based on a circular pipe.

$$D = \frac{2\,(endgap)(edge)}{endgap + edge} \tag{4.14}$$

Drawing the control volume and applying a fluid statics analysis to it as shown in Figure 4.6 yields

$$(p\,l)\pi r^2 - (p\,l - \Delta p)\pi r^2 - (\tau)2\pi r\ell = 0 \tag{4.15}$$

$$=>\frac{\Delta p}{\ell} = \frac{2\tau}{r} \tag{4.16}$$

where the acceleration is zero during fully developed flow when the velocity is constant.

Equation 4.16 represents the basic balance in forces needed to drive each fluid particle along the channel in the ring gap with constant velocity. Since neither Δp nor ℓ are functions of the radial coordinate, r, it follows that $\frac{2\tau}{r}$ must be independent of r. Hence, it can be concluded that

$$\frac{\tau}{r} = Constant$$

Applying the boundary conditions

$\tau = 0$ at $r = 0$ and $\tau = \tau_w$, wall shear stress at $r = D/2$

$$\Rightarrow \tau = \frac{2\tau_w r}{D} \tag{4.17}$$

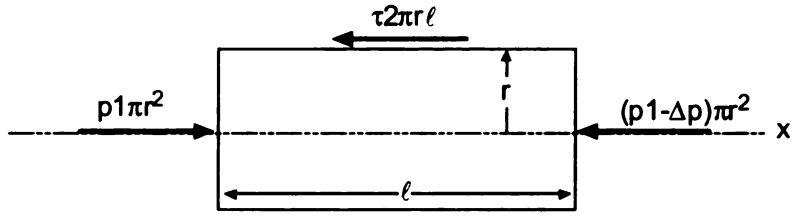

FIGURE 4.6 Free-Body Diagram of A Cylinder Fluid

From Equation 4.16 and Equation 4.17, the pressure drop and wall shear stress are related by

$$\Delta p = \frac{4\ell\tau_w}{D} \tag{4.18}$$

For laminar flow of a Newtonian fluid, the shear stress is proportional to the velocity gradient. In the notation associated with ring gap channel flow, the relationship is

$$\tau = -\mu\frac{du}{dr} \tag{4.19}$$

The negative sign is included to give $\tau > 0$ with $du/dr < 0$ (the velocity decreases from the centerline of channel to the wall.) Neglecting the gravitational effect, Equation

4.16 and Equation 4.19 are the two governing laws for a fully developed laminar flow of a Newtonian fluid. Combining these two equations, we obtain

$$\frac{du}{dr} = -\left(\frac{\Delta p}{2\mu\ell}\right)r \tag{4.20}$$

and we integrate it to give the velocity profile

$$\int du = -\frac{\Delta p}{2\mu\ell}\int r dr$$

or

$$u = -\left(\frac{\Delta p}{4\mu\ell}\right)r^2 + C1$$

where $C1$ is a constant. Applying boundary condition where $u = 0$ at $r = D/2$, yields

$$C1 = \left(\frac{\Delta p}{16\mu\ell}\right)D^2$$

$$u(r) = \left(\frac{\Delta p D^2}{16\mu\ell}\right)\left[1 - \left(\frac{2r}{D}\right)^2\right] \tag{4.21}$$

The maximum velocity is the centerline velocity, $Vc = \Delta p D^2/16\mu\ell$. The flowrate can be obtained by integrating the velocity with the cross-sectional area

$$Q = \int u dA = \int u(r) 2\pi r dr \tag{4.22}$$

$$Q = \frac{\pi D^2 Vc}{8} \tag{4.23}$$

By definition, the average velocity is the flowrate divided by the cross-sectional area, $V = Q/A$, so that for this flow

$$V_{ave} = \frac{\pi D^2 Vc}{8}\left(\frac{4}{\pi D^2}\right) = \frac{Vc}{2} = \frac{\Delta p D^2}{32\mu\ell} \tag{4.24}$$

and

$$Q = \frac{\pi D^4 \Delta p}{128\mu\ell} \tag{4.25}$$

Equation 4.25 represents the formula for fully developed laminar flow of oil through the top compression ring gap where

Q volume flow rate of oil through ring gap

D hydraulic diameter of ring gap channel

Δp pressure difference between the second land of ring pack and combustion chamber

μ viscosity of engine oil

ℓ ring width, the distance travelled by the oil flow

4.4 Total Oil Consumption

Equation 4.1 and Equation 4.25 represent two formulas of the oil consumption mechanism: oil vaporization and reverse flow through ring gap. Adding the oil loss from

these two mechanisms allows the prediction of the total oil consumption during a specific time of engine operation.

$$Total\ Oil\ Consumption = Oil_{evap} + Oil_{rev} \tag{4.26}$$

In this thesis, it is assumed that vaporization and reverse oil flow are the only two sources of oil loss. This assumption is made for the purpose that one can study the behavior of oil consumption under the influence of vaporization and reverse flow through ring gap.

Chapter 5 SIMULATION ANALYSIS OF OIL CONSUMPTION AND PISTON RING WEAR IN A 4.6L,V8 ENGINE

5.1 Introduction

This chapter presents the results of a simulation analysis of the ring pack behavior, oil film thickness, oil consumption and ring wear, and focus mainly on the relationships among them. In this thesis, the developed computer programs, RING, TWIST, PISTON, WEAR and OILCONSUME were used in combination with an engine thermodynamic model, the Ford Motor Company General Engine Simulation (GESIM). RING, TWIST and PISTON are parts of the Cylinder kit Analysis System for Engines (CASE) while WEAR and OILCONSUME are programs developed to be implemented into the CASE.

RING is a model used to predict groove and inter-ring gas pressure in a piston ring pack for reciprocating gasoline and diesel engines. It also predicts the oil film thickness between piston and cylinder bore, and piston ring and cylinder bore. This program requires the description of the engine intended to be studied. PISTON is a model used to predict the piston tilt per engine cycle. TWIST is a model used to predict the piston ring twist behavior. WEAR is a model used to compute the amount of worn volume from the first compression ring surface for a complete cycle and it can be integrated for specified time interval. OILCONSUME is a model used to compute the oil consumption caused by vaporization and reverse flow.

The GESIM program is a computational tool used in the Ford ENGine SIMulation system (ENGSIM) to model in-cylinder processes in an IC engine. The simulation results

include in-cylinder flow, heat transfer, and pressure vs. crank angle during engine cycle. It accounts for heat transfer losses from the combustion chamber during intake, compression, expansion, and exhaust stroke for both burned and unburned gases during combustion.

5.2 Integration of Different Computer Models

For this analysis, GESIM was used to generate simulation data of a 4.6L V8 IC engine. The data include in-cylinder pressure, in-cylinder temperature, bore temperature, piston temperature and in-cylinder heat convection coefficient. The engine description and the generated data were the input for RING, TWIST, PISTON, WEAR and OILCONSUME. Data of oil film thickness, pressure load of compression ring, inter-ring gas pressure, ring twist and piston tilt were generated by RING, PISTON and TWIST. These data were input into WEAR and OILCONSUME. The results of simulation include blow-by, oil film thickness, oil consumption rate and wear rate. For this thesis, nine simulated cases were selected as shown in Table 5.1.

TABLE 5.1 Selected Simulation Cases

Case	Operating Condition
1	1600rpm WOT (0.0 inches manifold vacuum)
2	1600rpm 50.0% Load (12.0 inches manifold vacuum)
3	1600rpm 16.67% Load (20.0 inches manifold vacuum)
4	3200rpm WOT (0.0 inches manifold vacuum)
5	3200rpm 50.0% Load (12.0 inches manifold vacuum)
6	3200rpm 16.67% Load (20.0 inches manifold vacuum)
7	5000rpm WOT (0.0 inches manifold vacuum)
8	5000rpm 50.0% Load (12.0 inches manifold vacuum)
9	5000rpm 16.67% Load (20.0 inches manifold vacuum)

5.3 Engine Specification of A 4.6L-8 Cylinder IC Engine

The basic specification of the engine model used in this work is shown in Table 5.2.

TABLE 5.2 Engine Data

Parameter	**Specified Value**
Engine Speed	1600rpm, 3200rpm, 5000rpm
Load	16.67%(20 inHg), 50.0%(12 inHg), WOT(0 inHg)
Bore diameter	90.4 mm
Stroke	90.0 mm
Connecting rod length	150.7 mm
Connecting rod mass	577 g
Number of rings	Two compression rings and one 3-piece oil control ring
Piston diameter	90.2 mm
Piston height	56.4 mm
Piston mass	356 g
Upper Compression Ring Width	1.47 mm
Maximum Top Compression Ring Height	3.83 mm
Upper Compression Ring Mass	10.6 g
Upper Compression Ring Tension	24.0 N

The top compression ring has been divided into 9000 elements as shown in Figure 5.1. Each element is identified with Segment ID and Slice ID for the calculation and analysis purpose.

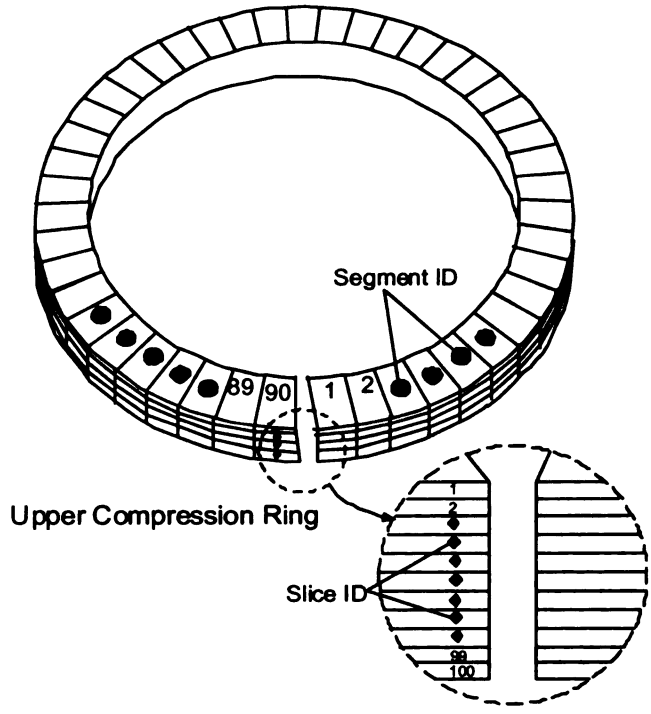

FIGURE 5.1 Identification Numbering for Piston Ring

5.4 Simulation Results

The results presented here is separated into two parts: comparison of results at different operating conditions of the engine and comparison of the transient results. It is important for one to notice the trend of each individual result affecting each other under the same or different conditions as time increases. It needs to be emphasized here that only the upper compression ring is considered in the wear analysis. The upper compression ring is the focus because of the most severe environment it is exposed to compared to the second ring and the oil ring.

5.5 Results and Discussions

5.5.1 Cylinder Pressures

The cylinder gas pressures versus engine crank angle for all simulated cases are shown in Figure 5.2. Comparing the cylinder pressures at 1600rpm (Figure 5.3), 3200rpm (Figure 5.4), and 5000rpm (Figure 5.5) indicated that the engine speed did not significantly affect the magnitude of the cylinder peak pressure. However, the engine load had significant effect on the peak pressure. Higher cylinder peak pressure was observed at higher engine load. For all three engine speeds, 1600rpm, 3200rpm and 5000rpm, the highest cylinder peak pressure was observed at 0.0 inch manifold vacuum (100% load), and the lowest at 20.0 inch manifold vacuum (16.67% load). The cylinder pressure peaked at about 365 degree crank angle, due to the fuel ignition during the power stroke.

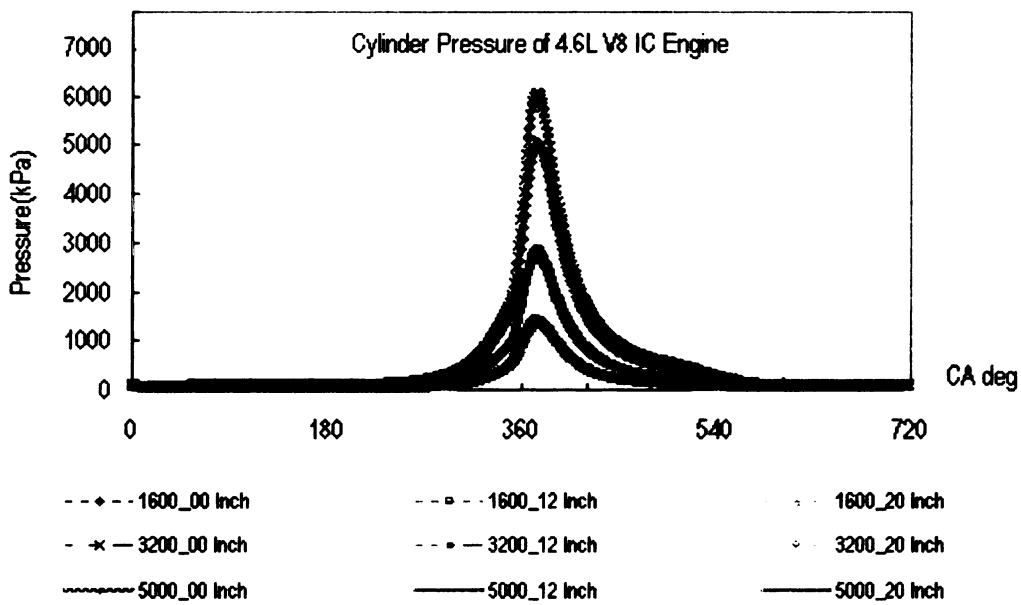

FIGURE 5.2 Cylinder Pressure at Different Operating Conditions

Images in this thesis are presented in color

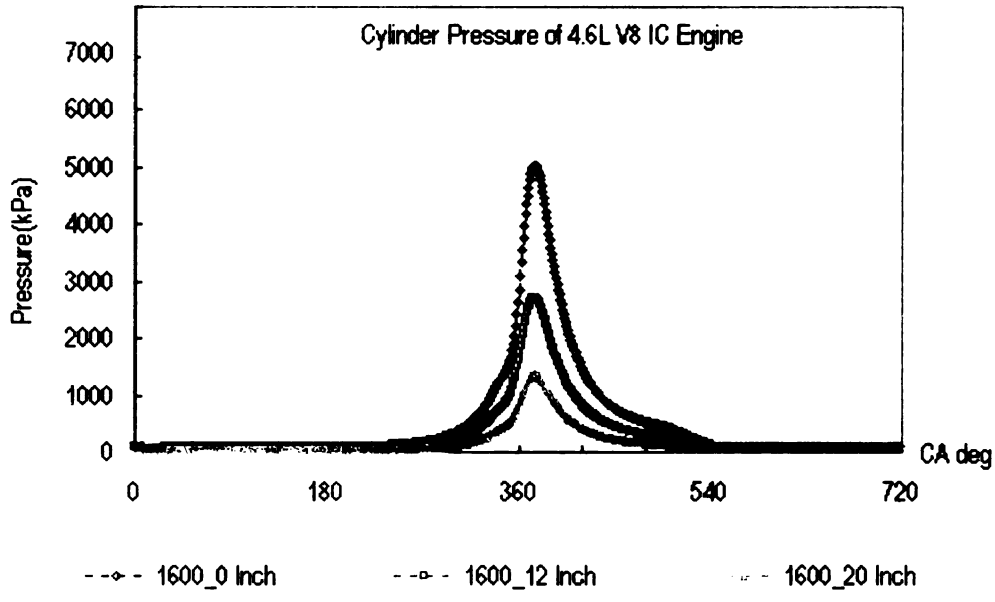

FIGURE 5.3 Cylinder Pressure at 1600rpm

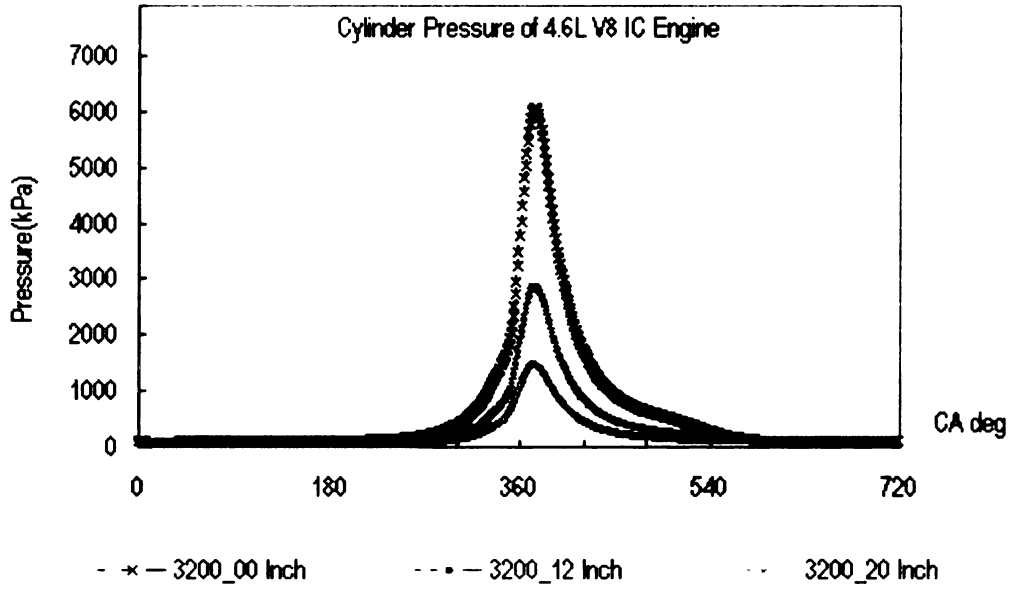

FIGURE 5.4 Cylinder Pressure at 3200rpm

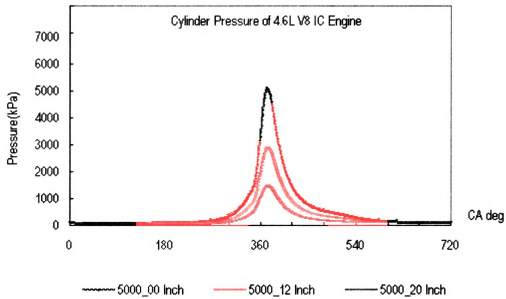

FIGURE 5.5 Cylinder Pressure at 5000rpm

5.5.2 Oil Film Thickness

The cylinder pressures influence the piston ring pack dynamics including the oil film formation. Using RING, the oil film thickness results were generated. The comparison of the predicted oil film thickness for different simulated cases (1600rpm 0.0 inch, 1600rpm 12.0 inch, 1600rpm 20.0 inch, 3200rpm 0.0 inch, 3200rpm 12.0 inch, 3200rpm 20.0 inch, 5000rpm 0.0 inch, 5000rpm 12.0 inch, 5000rpm 20.0 inch manifold vacuum) was shown in Figure 5.6. The oil film reached its maximum value when the piston was approaching TDC. At a same engine load, the highest maximum oil film thickness was observed at 5000rpm, and the lowest at 1600rpm. On the other hand, at a same engine speed, the highest maximum oil film thickness was observed at 20.0 inch manifold vacuum, and the lowest maximum oil film was at 0.0 inch manifold vacuum. For this engine, with only the speed and the load varied, the minimum oil film thickness

values for all operating conditions were the same at about 1.40μm. This result concluded that increasing the engine speed and reducing the engine load can increase the overall oil film thickness. In general, sufficient thickness of the oil film is necessary at high engine speed and high load to ensure efficient lubrication system.

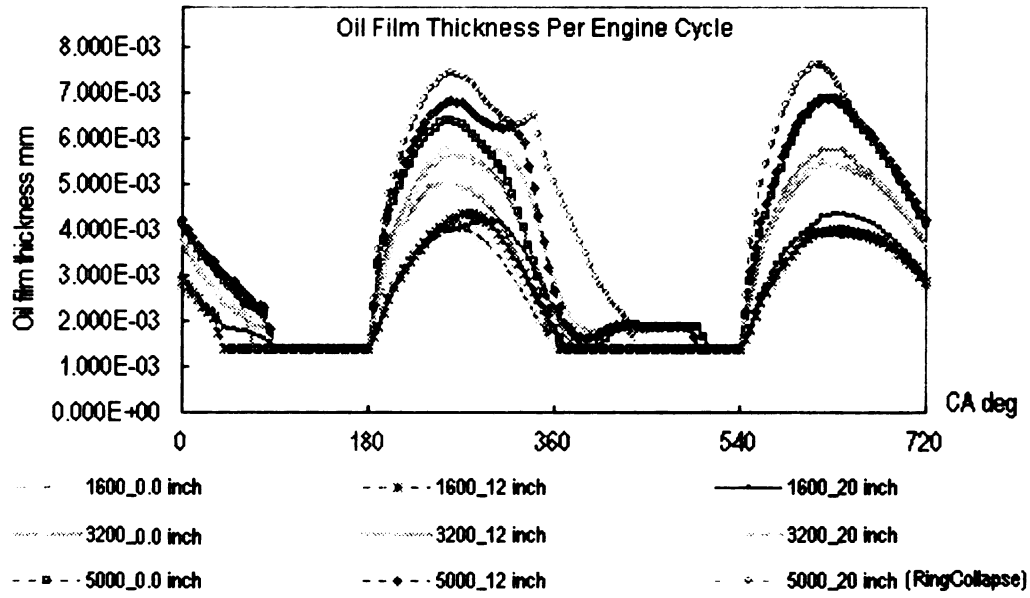

FIGURE 5.6 Predicted Oil Film Thickness (1st Cycle)

The transient analysis was performed for the oil film thickness. Comparing the transient results at 1600rpm 0.0 inch (Figure 5.7), 3200rpm 0.0 inch (Figure 5.8) and 5000rpm 0.0 inch manifold vacuum (Figure 5.9) showed that, over the simulation period of 500 hours, the oil film thickness varied at different degree in magnitude under different engine speeds and loads. The greatest change of the oil film formation was observed at the operating condition of 5000rpm 0.0 inch manifold vacuum in comparison with other cases. This is because under this condition, the piston ring face underwent the most severe deformation (discussed in the later section). However, the variation of oil film thickness

over the simulation period was small as shown in Figures 5.7, 5.8 and 5.9. This indicates that the oil film formation may not be sensitive to the worn piston ring face profile. This can be due to the limitation of the input data line in describing the piston ring face profile for RING program simulation.

Note: The simulation using RING program predicted the ring collapse at the initial operating condition of 5000rpm 20 inch-manifold. Since the ring collapse phenomenon violates some assumptions in analysis, this operating condition was eliminated from simulations discussed in the following sections.

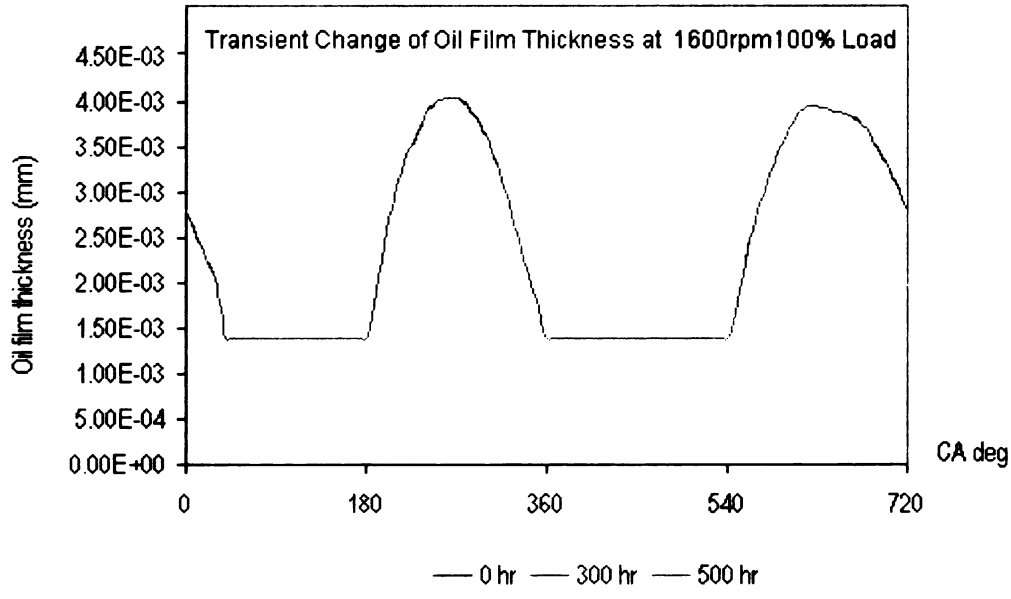

FIGURE 5.7 Oil Film Development at 1600rpm 0.0 inch Manifold Vacuum

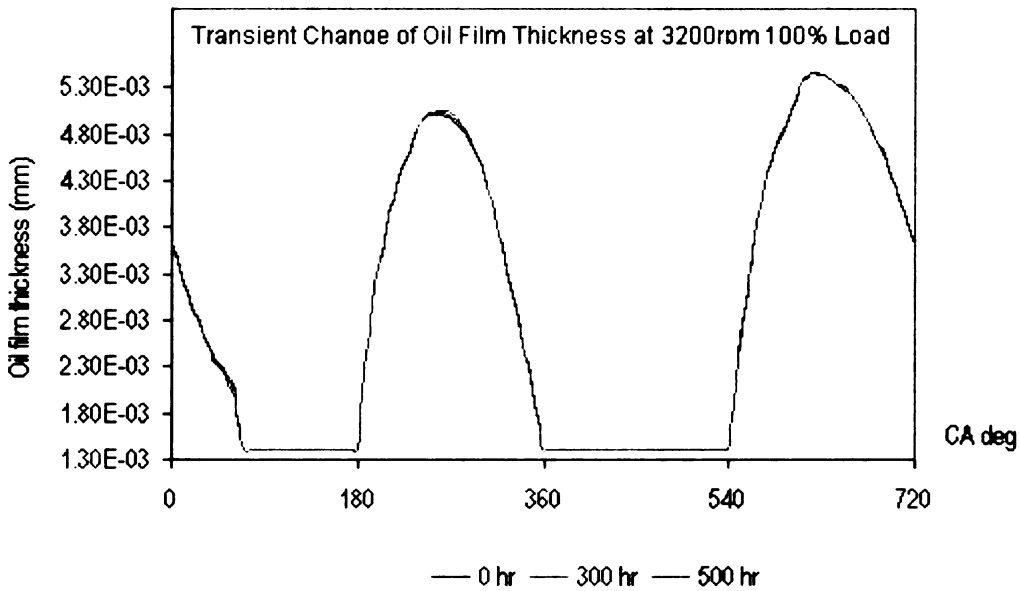

FIGURE 5.8 Oil Film Development at 3200rpm 0.0 inch Manifold Vacuum

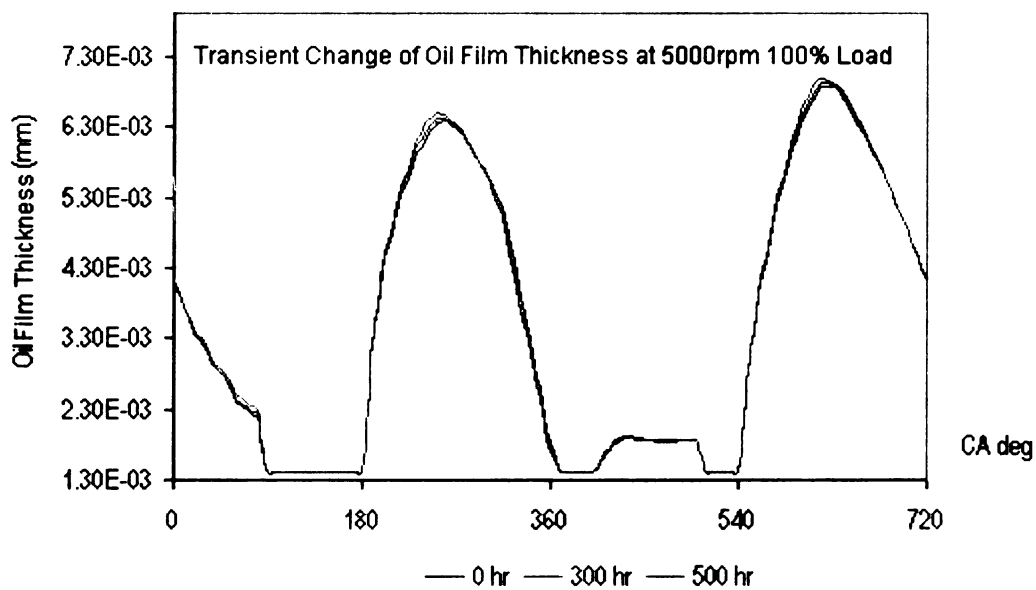

FIGURE 5.9 Oil Film Development at 5000rpm 0.0 inch Manifold Vacuum

5.5.3 Average Blow-by

It is important to examine the blow-by of the engine under different operating conditions because the blow-by tells the effectiveness of the piston ring pack in controlling mass flow within the cylinder kit. RING was used to generate the blow-by results. Figure 5.10 shows the average blow-by obtained after the first cycle of simulation. The highest blow-by was observed at 5000rpm 0.0 inch manifold vacuum, where the engine experienced the highest speed and load. The lowest blow-by was observed at 1600rpm 20.0 inch manifold vacuum. This can conclude that increasing both the engine speed and the engine load will increase the blow-by proportionally.

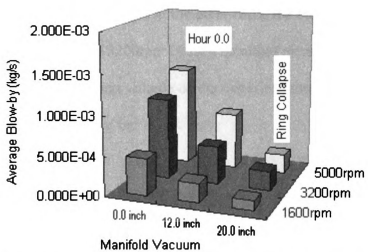

FIGURE 5.10 Prediction of Average Blow-by (Hour 0.0)

In order to study the effect of the piston ring wear and the oil consumption on the blow-by, the average blow-by after 500 hours of simulation was obtained for all simulated cases, as shown in Figure 5.11. Comparing Figure 5.10 and Figure 5.11 showed a significant increase of blow-by over the 500 hours of simulation. The increase of the average blow-by ranged from 3.0% at 3200rpm 20.0 inch to 50.0% at 5000rpm 0.0 inch

manifold vacuum (Figure 5.12). The increase of the blow-by may depend on the degree of deformation experienced by the ring surface, as shown in Figure 5.34, Figure 5.35 and Figure 5.36. Generally, the functionality of the ring face relies on the piston ring face profile and the ring dimension. The wear caused the deformation on the ring face as well as the reduction of the ring width. This increased the inter-ring volume in which the blow-by was evaluated on. The transient wear analysis in the later part of this chapter showed that the piston ring underwent the most severe change under the operating condition of 5000rpm 0 inch manifold pressure, in which the maximum ring width was reduced by 14%. The 14% reduction of the maximum ring width had contributed to 50% increase in the inter-ring volume (groove and land volume) of upper compression ring, which was in proportion to the increase of blow-by. On the other hand, the reduction of the ring width was 0.8% under the condition of 3200rpm 20 inch manifold pressure, and it contributed to the 3.0% increase of the inter-ring volume of the upper compression ring, which was in proportion to the increase of blow-by.

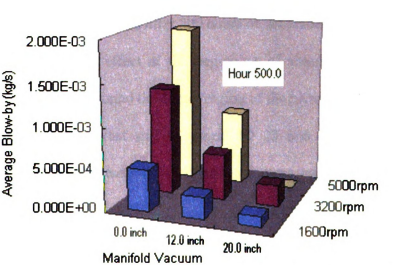

FIGURE 5.11 Prediction of Average Blow-by (Hour 500.0)

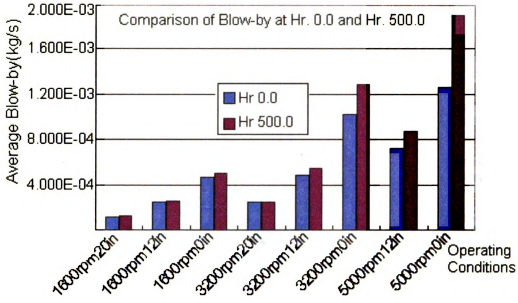

FIGURE 5.12 Comparison of Average Blow-by Increase

5.5.4 Piston Ring Wear

WEAR was used to generate the distribution of wear on the piston ring surface, the transient change of the ring profile affected by the wear, and the wear rate over the period of simulation. Comparing the wear distribution at 1600rpm 0.0 inch manifold vacuum after the first cycle (Figure 5.13) and after 500 hours of simulation (Figure 5.14) yield two observations. First, the wear effect at the beginning of simulation (Figure 5.13) was observed to be concentrated around the center region of the piston ring (Slice ID 40 to 60) and at the thrust and anti-thrust side (Segment ID 23 and 68). After 500 hours of simulation (Figure 5.14), the wear effect distributed more evenly over the piston ring surface.

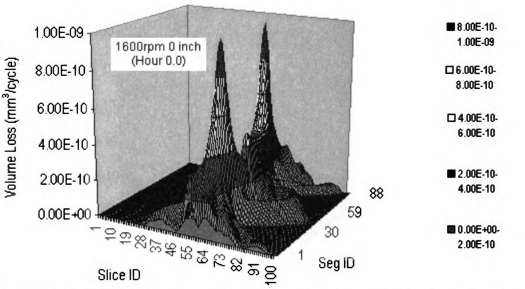

FIGURE 5.13 Wear at 1600rpm 0.0inch Manifold Vacuum(1st Simulation Cycle)

Second, the magnitude of the maximum wear volume decreased (80%) over the 500 hours of simulation. When the piston ring surface underwent the deformation, greater area on the piston ring surface were experiencing the wear effect. With greater surface area against the reacting forces from the cylinder bore, less stress was experienced by each divided surface element on the piston ring (since stress is force divided by area). As a result, the magnitude of the maximum wear volume was observed to decrease.

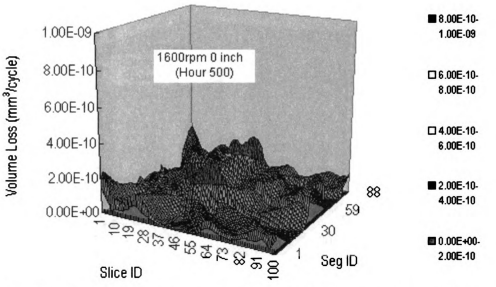

FIGURE 5.14 Wear at 1600rpm 0.0inch Manifold Vacuum (After 500 hours)

Similar analysis was performed for lower engine loads at 1600rpm. Figures 5.15 and 5.16 are the wear distribution plots for 1600rpm 12 inch manifold vacuum, after the first cycle and after 500 hours of simulation respectively. Figures 5.17 and 5.18 are the plots for 1600rpm 20 inch manifold vacuum. Comparing the wear distribution plots of different engine loads at 1600rpm showed that the magnitude of the maximum wear volume decreased as the engine load decreased. The highest magnitude of wear volume was observed at 100% load and the lowest at 16.67% load.

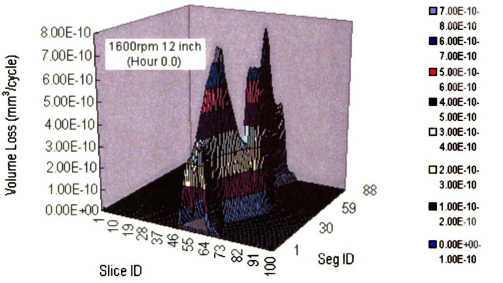

FIGURE 5.15 Wear at 1600rpm 12.0inch Manifold Vacuum(1st Simulation Cycle)

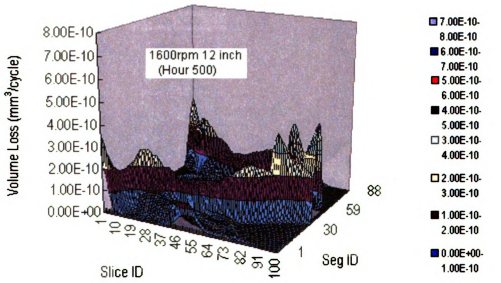

FIGURE 5.16 Wear at 1600rpm 12.0inch Manifold Vacuum (After 500 hours)

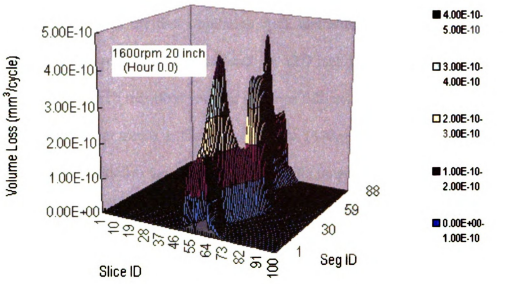

FIGURE 5.17 Wear at 1600rpm 20.0inch Manifold Vacuum(1st Simulation Cycle)

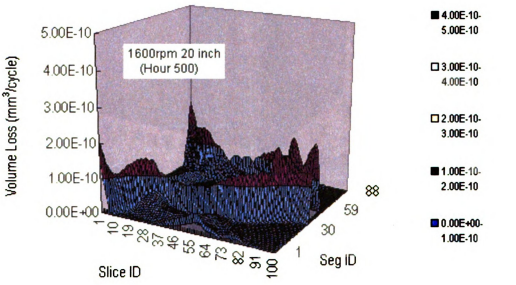

FIGURE 5.18 Wear at 1600rpm 20.0inch Manifold Vacuum (After 500 hours)

Figures 5.19 and 5.20 are the wear distribution plots for 3200rpm 0.0 inch at two different time periods, after the first simulation cycle and after 500 hours of simulation. Comparing with the lower load conditions such as 12.0 inch manifold vacuum (Figures 5.21 and 5.22) and 20 inch manifold vacuum (Figures 5.23 and 5.24) at the same engine speed of 3200rpm, similar trends as the wear results at 1600rpm were also observed. The wear distribution was initially concentrated at the middle range of the piston ring surface, and later distributed more evenly over the surface at lower magnitude.

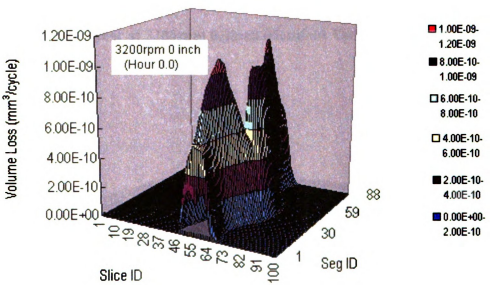

FIGURE 5.19 Wear at 3200rpm 0.0inch Manifold Vacuum(1st Simulation Cycle)

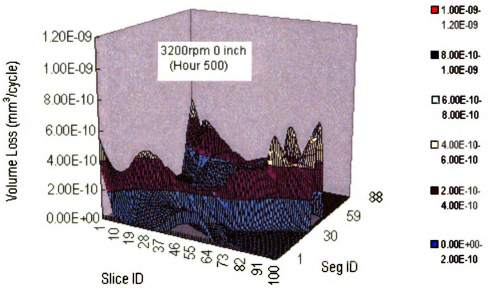

FIGURE 5.20 Wear at 3200rpm 0.0inch Manifold Vacuum(After 500 hours)

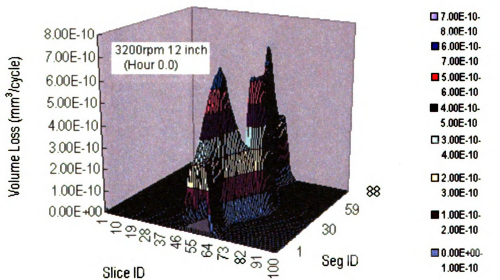

FIGURE 5.21 Wear at 3200rpm 12.0inch Manifold Vacuum(1st Simulation Cycle)

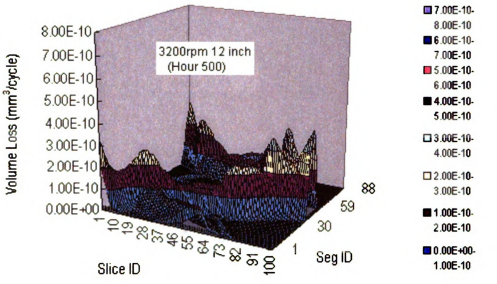

FIGURE 5.22 Wear at 3200rpm 12.0inch Manifold Vacuum(After 500 hours)

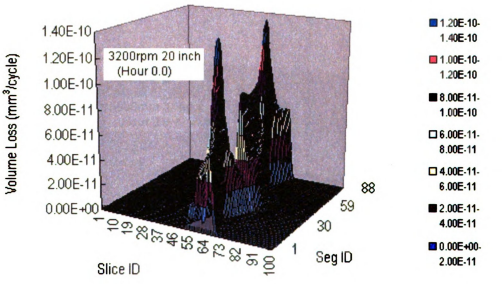

FIGURE 5.23 Wear at 3200rpm 20.0inch Manifold Vacuum(1st Simulation Cycle)

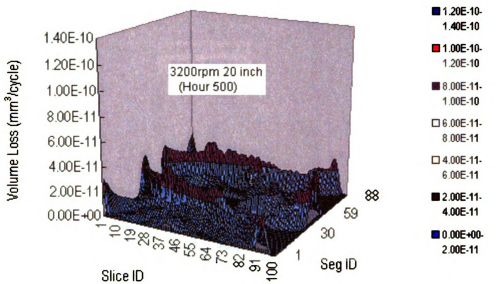

FIGURE 5.24 Wear at 3200rpm 20.0inch Manifold Vacuum(After 500 hours)

The wear analysis for the engine speed of 5000rpm also gave similar observations as discussed previously for 1600rpm and 3200 rpm. Figures 5.25 and 5.26 are the plots for 5000rpm 0.0 inch, and Figures 5.27 and 5.28 for 5000rpm 12 inch manifold pressure.

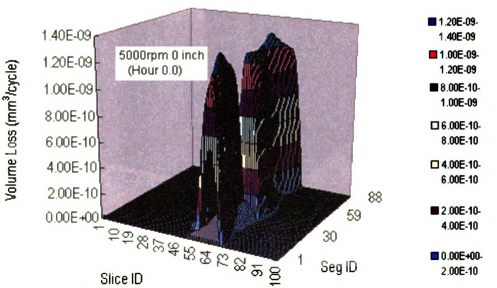

FIGURE 5.25 Wear at 5000rpm 0.0inch Manifold Vacuum(1st Simulation Cycle)

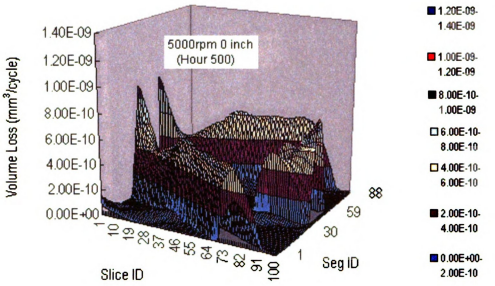

FIGURE 5.26 Wear at 5000rpm 0.0inch Manifold Vacuum(After 500 hours)

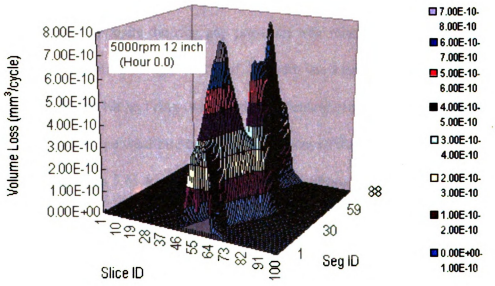

FIGURE 5.27 Wear at 5000rpm 12.0inch Manifold Vacuum(1st Simulation Cycle)

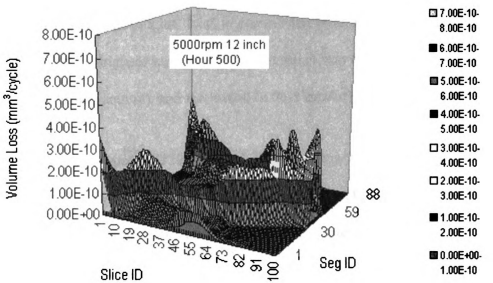

FIGURE 5.28 Wear at 5000rpm 12.0inch Manifold Vacuum(After 500 hours)

In order to study the transient characteristic of the piston ring wear, simulation was performed over 500 hours of simulation period to obtain the piston ring wear rate. Since different locations on the piston ring surface have different wear effect, the elements on Segment ID of 45 (opposite the ring gap position) was selected for the wear rate to be obtained. The elements on Segment ID of 45 were the elements that experienced less effect from the piston tilt and ring twist so that the calculation of the wear rate would be more stable. The average wear rate taken from all slices of Segment ID of 45 were plotted in Figures 5.29 through 5.31 for different operating conditions.

Figure 5.29 shows the wear rate at 1600rpm under different engine loads. It was observed that the wear rate of each operating condition decayed to their steady state values at different time periods. The wear rate of 1600rpm 0.0 inch manifold vacuum reached its steady state value after about 100 hours, 1600rpm 12.0 inch manifold vacuum about 150

hours, and 1600rpm 20 inch manifold vacuum about 250 hours. In addition, it was observed that increasing the engine load increased the wear rate during steady state. During steady state, the highest wear rate (1.9e-4 mm/hr) was observed at 100% engine load (0.0 inch manifold vacuum), and the lowest (8.0e-5 mm/hr) at 16.67% engine load.

At higher engine speeds, 3200rpm and 5000rpm, the wear rates under different engine loads were plotted in Figures 5.30 and 5.31 respectively. Comparing the wear rates of 3200rpm shown in Figure 5.30 showed that the wear rate of each engine load also decayed to their steady state values at different time periods. The settling time periods for 3200rpm 0.0 inch, 12.0 inch and 20 inch manifold pressure were about 30 hours, 60 hours and 100 hours respectively. From Figure 5.31, it was noticed that the settling time periods of the wear rate were 20 hours and 40 hours for 5000rpm 100% load and 50% load respectively.

It is interesting to note that the wear rates at the lower loads of each engine speed stabilized at a level coincidentally lower than the other engine loads. The possible explanation is that at lower engine load, the combined stress experienced by the piston ring surface is low due to the low cylinder peak pressure (refer to Figure 5.2).

The decrease of the wear rate can also be explained using the Abbott Firestone Curve in addition to the stress analysis discussed earlier in this section. Refer to the Abbott Firestone Curve shown in Figure 3.5 in Chapter 3. Under the wear effect, the peaks of the piston ring surface were reduced. This resulted in the increase of the bearing ratio. At the microscopic scale, the increase of the bearing ratio means more real contact surface exists

between the piston ring face and the cylinder liner. The increase of the real contact surface results in the reduction of stress (stress is force divided by area) because more surface asperities are bearing the contact force at the same time. The decrease of the stress will result in the decrease of the wear according to the wear formulation.

The steady-state wear rates in Figure 5.29(1600rpm), Figure 5.30(3200rpm) and Figure 5.31(5000rpm) were compared (Figure 5.32) in order to draw an observation associating the wear rate to the engine speed and load. It was observed that during the steady state, increasing the engine load would result in the increase of the wear rate. However, increasing the engine speed would not ensure the increase of the wear rate, as shown in Figure 5.32. At the 16.67% load, rising the engine speed from 1600rpm to 3200rpm resulted in the reducing of the steady-state wear rate. This observation can be explained using the oil film thickness analysis. It was discussed previously that increasing the engine speed would increase the maximum oil film thickness. The increase of the maximum oil film thickness ensured the occurrence of hydrodynamic lubrication, which prevents wear. Based on this argument, it can be understood that the piston ring wear could be reduced by increasing the engine speed(low range of engine speed), for the same engine power output. This observation agrees with observation from Chung's results[1], which showed the increase of wear rate when the engine speed increased from 1200rpm to 2100rpm.

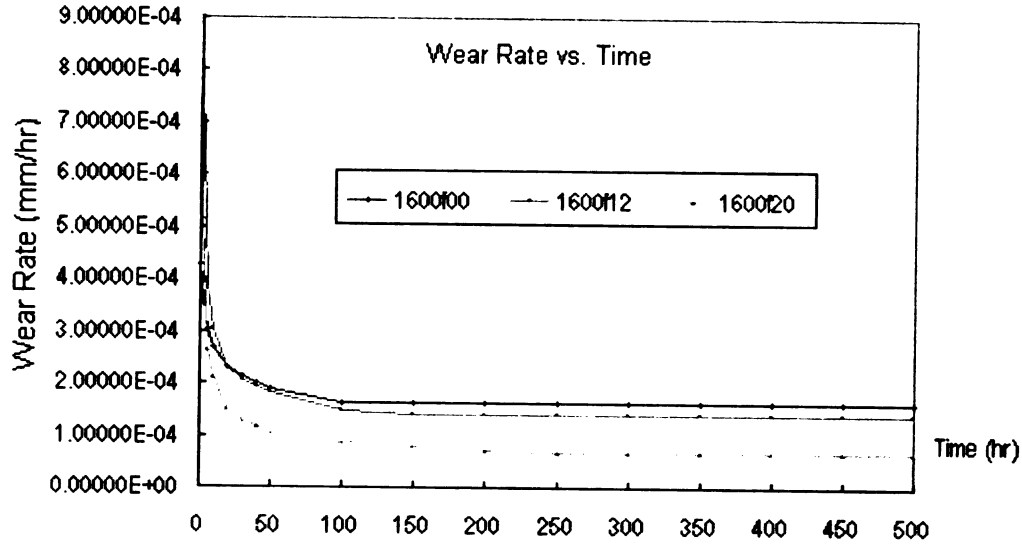

FIGURE 5.29 Wear Rate at 1600rpm

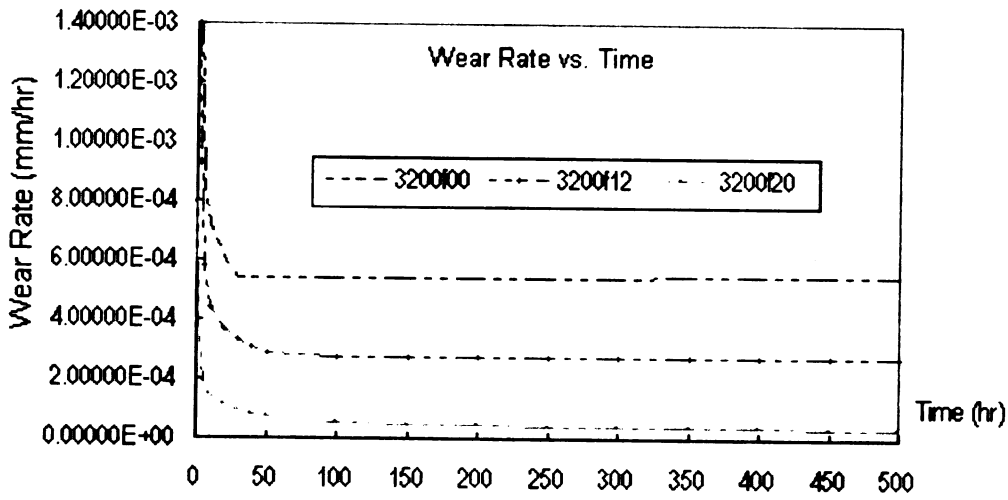

FIGURE 5.30 Wear Rate at 3200rpm

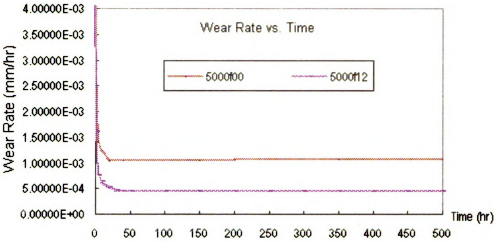

FIGURE 5.31 Wear Rate at 5000rpm

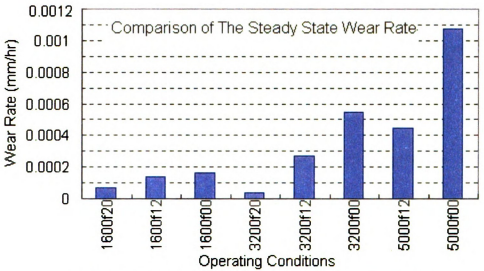

FIGURE 5.32 Comparison of Steady State Wear Rate

Experimental results from Barkman[2] showed a similar trend in the measured wear rate as displayed in Figure 5.33. The measurement of the piston ring wear rate was performed on a single cylinder engine using radiotracer-based wear diagnostic method. The wear rate decreased to a steady state value within 20 hours of simulation. A step input at the 25th hour of operation increased the wear rate quickly, but the wear rate returned to a steady state value within 10 hours.

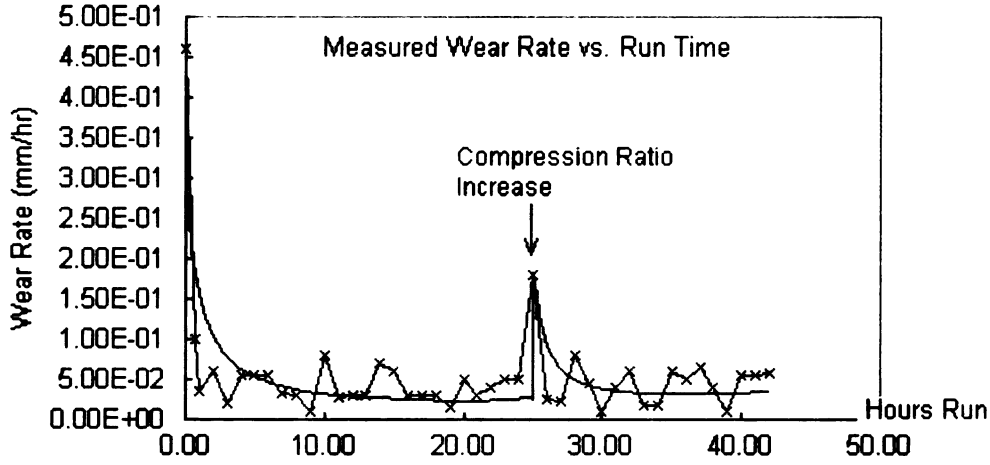

FIGURE 5.33 Measured Wear Rate

Besides the wear distribution and the wear rate analyses, the effect of the wear on the piston ring face profile is also presented in this section. The following figures display the change of the cross-sectional ring face profile in 3-D(left) and 2-D(right) views for different simulated cases. The 45th segment of the piston ring was selected for this analysis. The 2-D plot shows the cross section of the piston ring profile at the 45th segment where the x-axis is the ring width and the y-axis the ring height. The legend of the 2-D plot contains the curves for the ring face profile at different time period during the simulation. The 3-D plot has the same description as the 2-D except with the time reference on the z-axis.

The 2-D and 3-D views of the transient change of upper compression ring face profiles at 45th Segment ID are displayed in Figures 5.34 through 5.36. Figure 5.34 show how the ring face profile evolve over the period of simulation at 1600rpm. It was observed that higher engine load caused greater deformation on the piston ring profile. Indeed, this observation was already expected from the wear rate analysis presented in previous

section. It was also observed that the ring face profiles for all simulated cases changed from the original parabolic-shaped to linear taper-shaped.

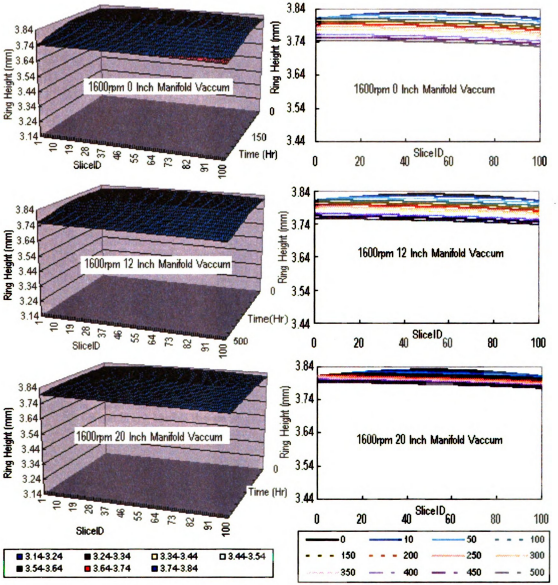

FIGURE 5.34 Ring Race Change at 1600rpm

Figure 5.35 shows evolvement of the piston ring face profile at 3200rpm. Similar to the simulation at 1600rpm, as expected, the degree of deformation was directly affected by the engine load. The most severe deformation occurred at the 100% load, and the least

at 16.67% load. As discussed in the wear rate analysis, the least deformation was observed at 3200rpm 16.67% compared to all other simulated cases at different loads and speeds.

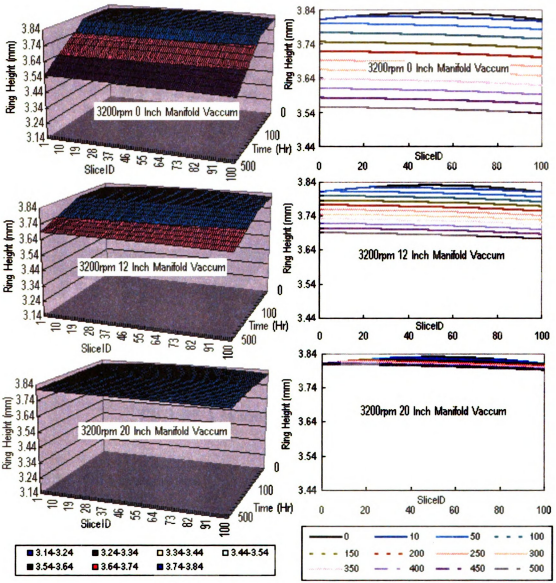

FIGURE 5.35 Ring Face Change at 3200rpm

Figure 5.36 shows the plots of the change of the piston ring profile at 5000rpm. As expected by the wear rate analysis, the most severe deformation occurred under the operating condition of 5000rpm 100% load in comparison with the simulated cases at 1600rpm (Figure 5.34) and 3200rpm (Figure 5.35).

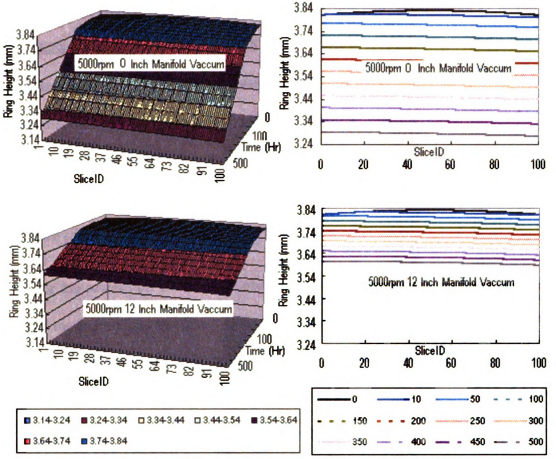

FIGURE 5.36 Ring Face Change at 5000rpm

5.5.5 Oil Consumption

The oil consumption mechanisms evaluated in this thesis are the oil vaporization and the reverse oil flow. Figure 5.37 showed the time-average oil consumption components of different operating conditions. It was observed that increasing the engine speed and reducing the engine load could increase the total oil consumption. The highest total oil consumption rate was observed at the operating condition of 5000rpm 12 inch-manifold pressure, while the lowest value was at 1600rpm 0.0 inch-manifold pressure.

For oil vaporization, it was observed that its rate increased when the engine speed increased and the engine load decreased. This observation can be explained by using the oil film thickness analysis. Comparing the oil film thickness result (Figure 5.6) with the oil vaporization result (Figure 5.37), it was observed that the effect of the speed and load on both the oil vaporization and the oil film thickness was the same. Since the oil vaporization was evaluated using the oil film thickness, the increase of the maximum oil film thickness (resulted from the increase the speed and the decrease the load) resulted in the increase of the oil vaporization, as shown in Figure 5.37.

For the reverse oil flow, it was observed that its rate decreased when the engine speed and the engine load increased. Comparing this results with the blow-by results gave an interesting observation: the effect of the engine speed and the engine load on the reverse oil flow is directly opposite from the effect on the blow-by (Figures 5.10, 5.11 and 5.12.) In contrast to the reverse oil flow, the blow-by increased when the engine speed and the engine load increased.

The blow-by is the flow of combustion gas from the combustion chamber into the engine crankcase, and its direction is opposite from the reverse oil flow. At high blow-by state, there is high flow rate of combustion gas across the piston ring pack in the direction from the combustion chamber to the engine crank. This means that the net pressure gradient per cycle across the piston ring pack is negative for the calculation of the reverse oil flow. As a result, the reverse oil flow per cycle was reduced.

Of the two oil consumption mechanisms studied, it was also observed that the oil vaporization was dominant at high speed (5000rpm) while the reverse oil flow was the

dominant oil loss component at low engine speed (1600rpm). The temperature data from GESIM showed that the average operational temperature per cycle is directly proportional to both engine speed and load. The higher the speed and load, the higher the operational temperature. The oil vaporization mechanism dominated at high speed means that the heat and mass transfer process with a concurrent high oil film thickness was playing a more important role during high engine speed operation (higher operational temperature), compared to lower engine speed operation (lower operational temperature.) The reverse oil flow dominates as the oil vaporization rate is much lower for the low speed conditions.

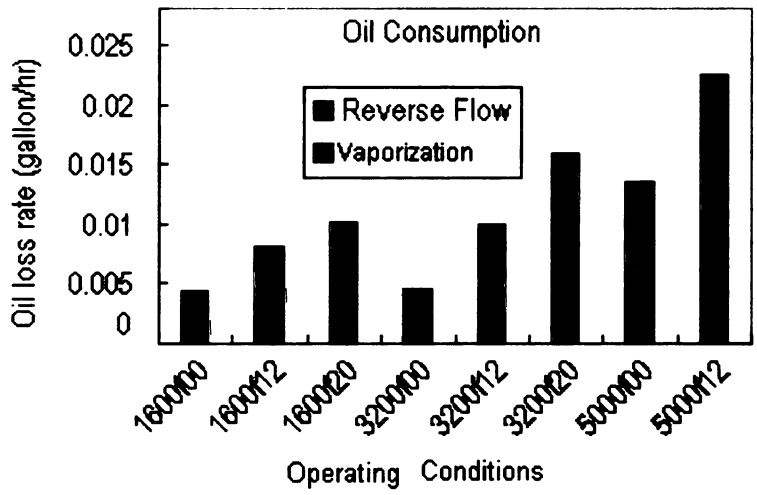

FIGURE 5.37Comparison of Time-average Oil Consumption over 500hrs Simulation

Wong et al. [8] performed the oil vaporization analysis using a computer simulation. Comparing the oil vaporization result obtained in this thesis, shown in Figure 5.38, with the result from Wong et al. [8] showed a good agreement. As mentioned in Chapter 1, Wong et al. [8] found that most (74%) of the oil vaporization occurred during the intake and compression strokes. The oil vaporization result in Figure 5.38 shows that

there was high percentage of oil vaporization during the intake and compression strokes of an engine cycle. Figure 5.38 shows that the lowest percentage (58%) of the oil vaporization occurred during the intake and compression strokes under the operating condition of 1600rpm 0.0 inch manifold vacuum, and the highest percentage (85%) under the operating condition of 3200rpm 20 inch manifold vacuum. The high percentage of vaporization during the intake and compression strokes was caused by the low oil vapor pressure and high convective coefficients that encourage heat and mass transfer process during these two strokes compared to the power and exhaust strokes.

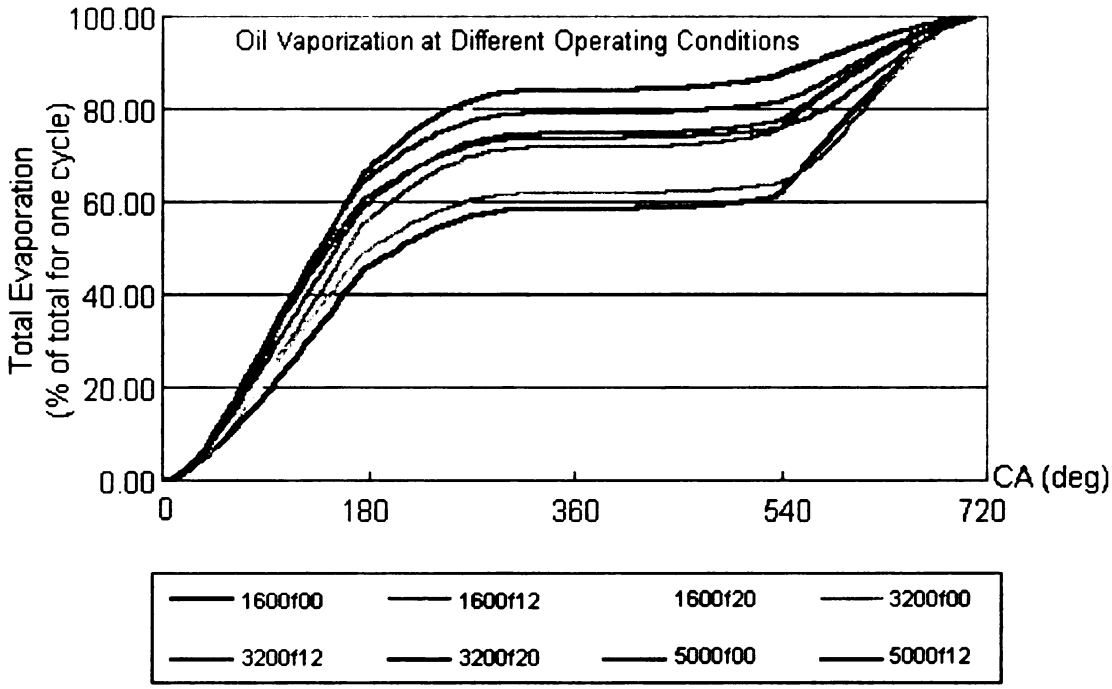

FIGURE 5.38 Estimated Oil Vaporization During One Cycle

Combining the reverse oil flow and oil vaporization gives the total oil consumption, as shown in Figure 5.39. The total oil consumption for all operating conditions underwent very small change over the period of simulation time. This observation was obtained since the transient results on the oil film thickness also

underwent small variation over the simulation period (refer to Figures 5.7 through 5.9). Moreover, the small effect of the worn ring surface on the overall ring pack pressure could also contribute to the small variation in the transient oil consumption results. Without including the wear effect on the piston ring tension, piston groove and cylinder bore, the ring pack pressure would not be significantly affected. As a result, the oil consumption rate, which is also evaluated using the ring pack pressure, did not have significant change over the simulation period.

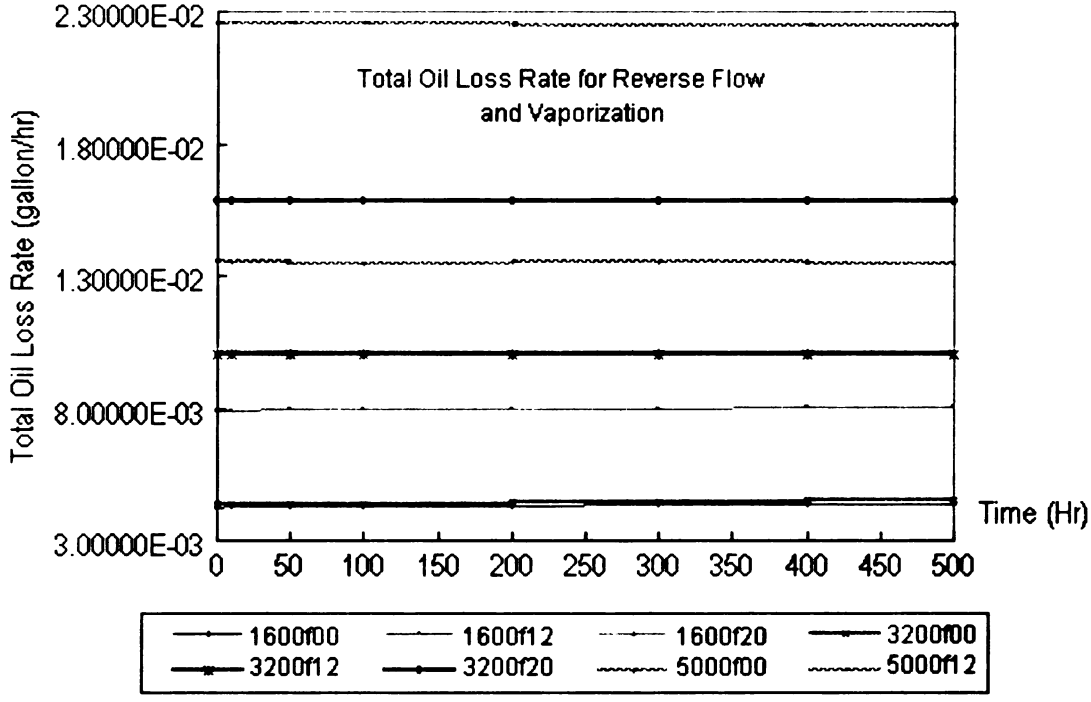

FIGURE 5.39 Total Oil Consumption Rate for Reverse Flow and Vaporization

5.5.6 Oil Consumption and Gas Back Flow

The relationship between the gas back flow and the oil consumption was also studied. The RING program was used to generate the gas back flow through the upper ring gap over 500 hours of simulation. The results of the oil consumption rate and the gas back flow for each simulated case were plotted in Figures 5.40 and 5.41. Figure 5.40 contains the plots of the oil consumption rate (using the left y-axis) and the back flow (using the right y-axis) for the first four cases: 1600rpm 0.0 inch, 1600rpm 12.0 inch, 1600rpm 20.0 inch and 3200rpm 0.0 inch manifold pressure. Figure 5.41 contains the plots for the other four cases: 3200rpm 12 inch, 3200rpm 20 inch, 5000rpm 0.0 inch and 5000rpm 12.0 inch manifold pressure. It was observed that a correlation existed between the gas back flow through the upper ring gap and the total oil consumption.

The transient change of the oil consumption rate and of the gas back flow was similar. When there was an increase in the gas back flow, there was also an increase in the oil consumption rate over the same period of simulation and vice versa. This correlation can be understood since the pressure difference of the piston ring pack is a driving force for both mechanisms. In addition, the flow of both mechanism are along the same path in the same direction, from the engine crank case to the combustion chamber. Thus, both mechanism showed a similar trend over the simulation period.

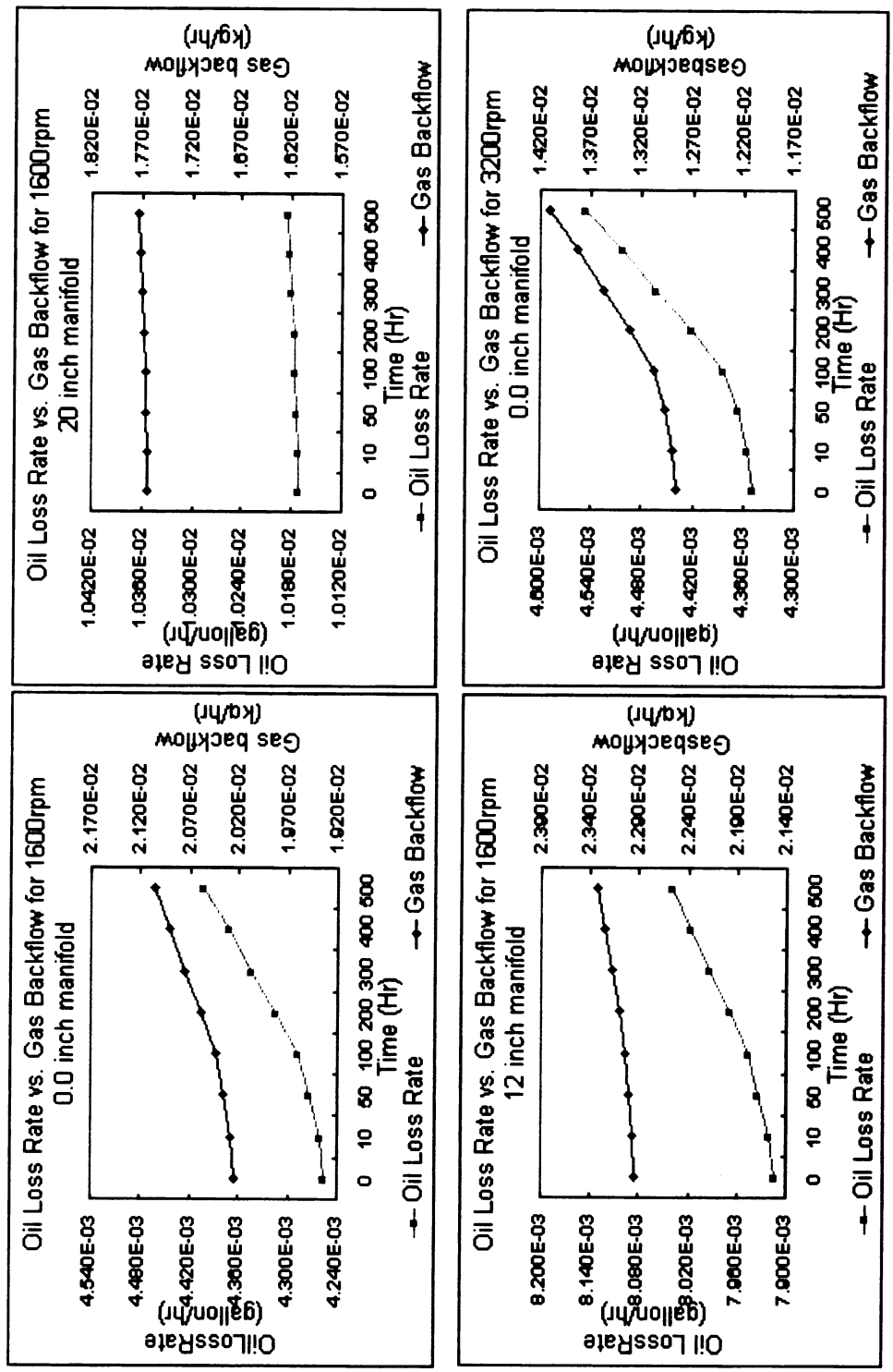

FIGURE 5.40 Oil Loss vs. Gas Backflow through 1st Ring Gap (I)

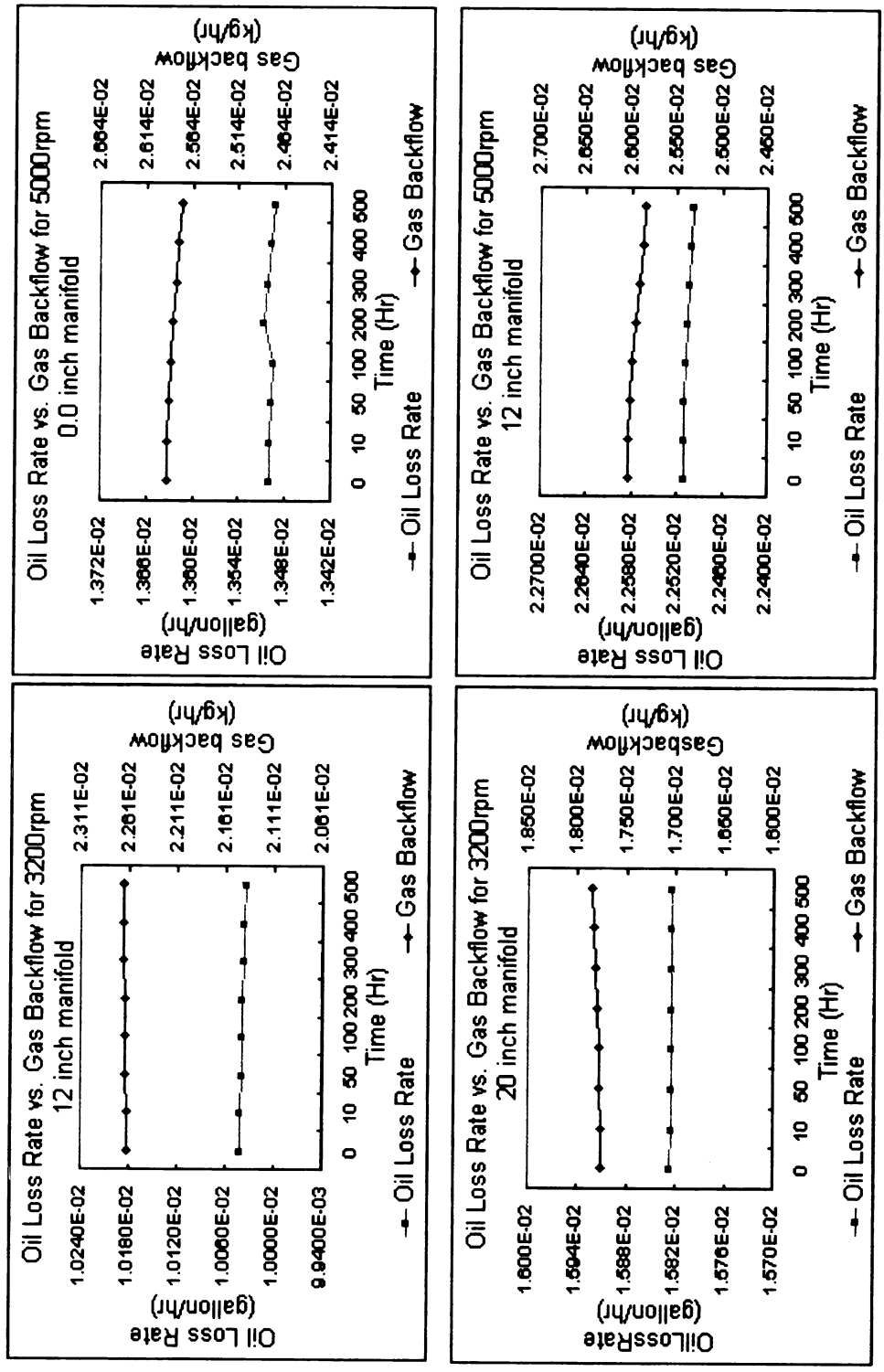

FIGURE 5.41 Oil Loss vs. Gas Backflow through 1st Ring Gap (II)

5.5.7 Oil Consumption and Average Gas Blow-by

The research on the relationship between the blow-by and the oil consumption was previously carried out at MSUERL by Ejakov [4]. This thesis carried out further investigation on how the blow-by relates to the oil consumption. The RING program was used to generate the blow-by over 500 hours of simulation. The plotting of the blow-by results with the oil consumption rate are shown in Figure 5.42 and Figure 5.43. Figure 5.42 contains the plots of the oil consumption rate (using the left y-axis) and the blow-by (using the right y-axis) for the first four cases: 1600rpm 0.0 inch, 1600rpm 12.0 inch, 1600rpm 20.0 inch and 3200rpm 0.0 inch manifold pressure. Figure 5.43 contains the plots for the other four cases: 3200rpm 12 inch, 3200rpm 20 inch, 5000rpm 0.0 inch and 5000rpm 12.0 inch manifold pressure.

It was observed that the oil consumption and the blow-by results underwent different trend of change over the simulation period depending on the engine speed. At 1600rpm, the oil consumption rate underwent relatively high increase over the simulation period, but the blow-by did not. At 5000rpm, the blow-by underwent relatively high increase but the oil consumption rate did not. However, at 3200rpm, the transient results of both mechanism were found to be correlated, in which the change of the blow-by was directly proportional to the change of the oil consumption.

With the limited number of cases performed in this work, no obvious conclusion could be drawn regarding the transient relationship between the blow-by and the oil consumption rate. This concept requires further study.

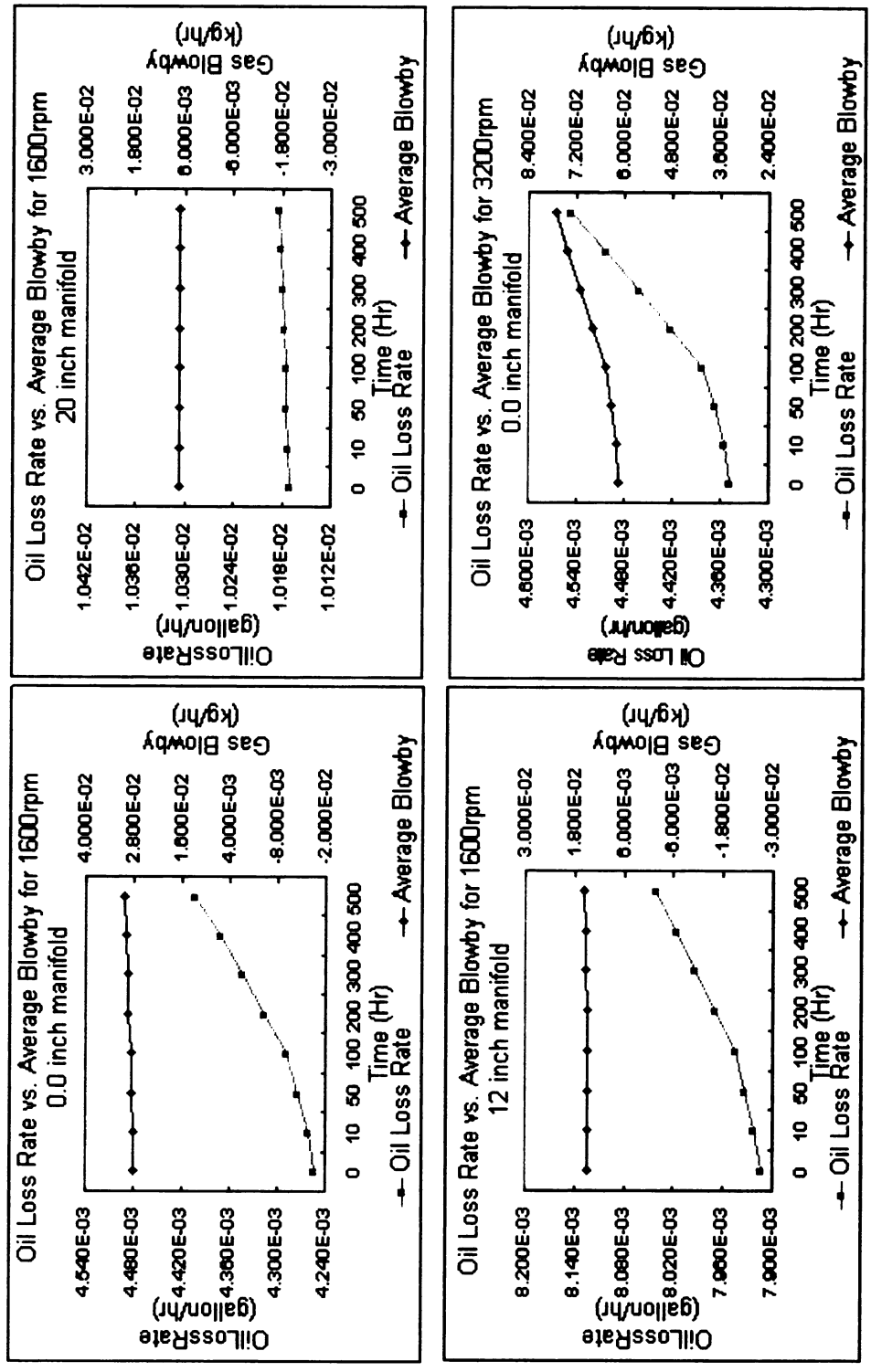

FIGURE 5.42 Oil Loss vs. Gas Blow-by (I)

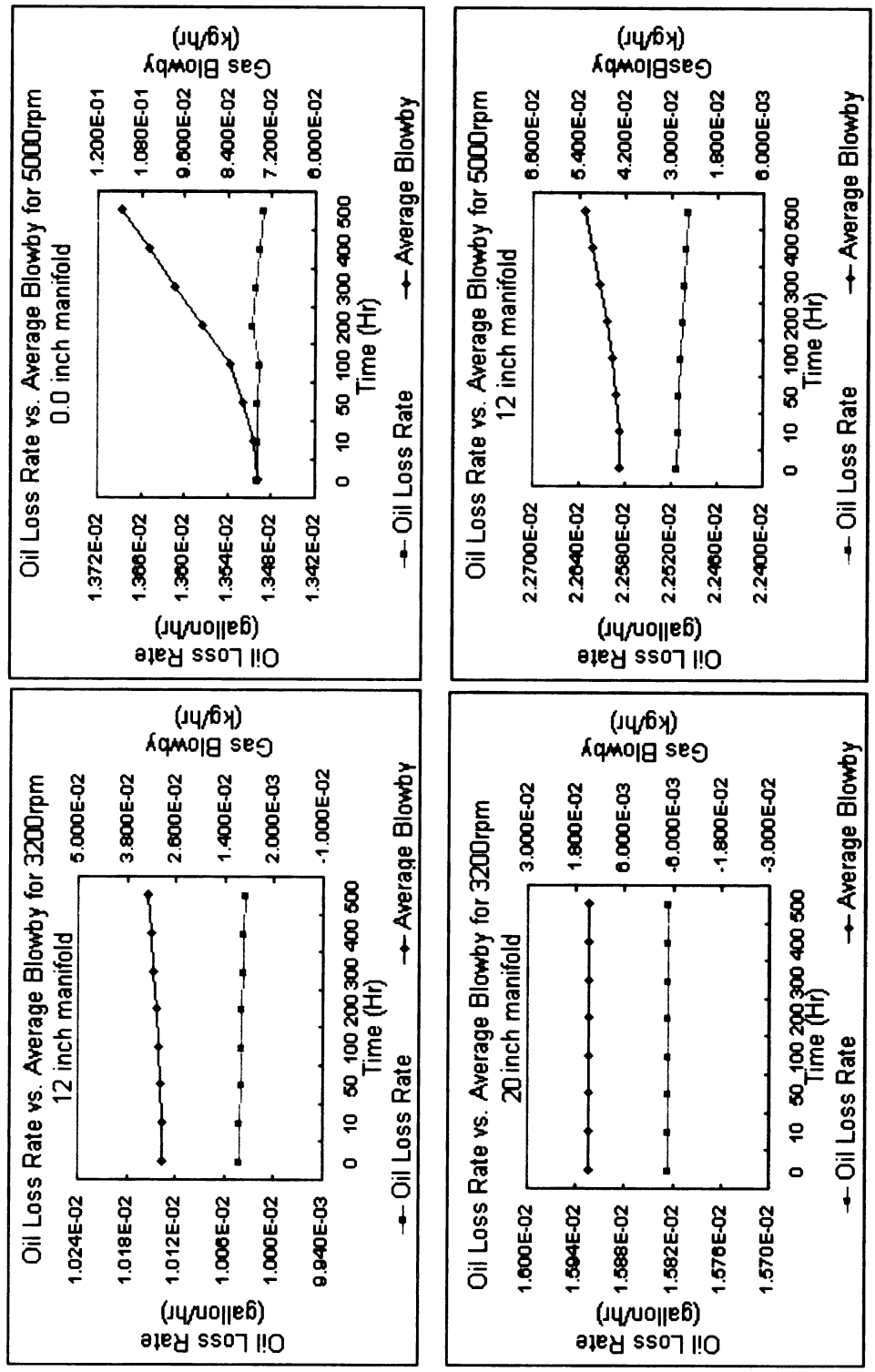

FIGURE 5.43 Oil Loss vs. Gas Blow-by (II)

5.5.8 Oil Consumption and Piston Ring Wear

The transient results of the wear rate and the oil consumption rate for each simulated cases were plotted in Figures 5.44 and 5.45. The number of simulation cases for this analysis is the same as the previous two analyses. The purpose for this analysis was to study how the oil consumption changed with respect to the wear rate.

First, it was observed that the oil consumption rate started to increase linearly when the wear rate was at steady state. Prior to steady state wear rate, the oil consumption rate increased non-linearly.

Second, the transition point decreased as the engine speed increased. At 1600rpm conditions, the change of the oil consumption trend from nonlinear to linear was at about the 100th hour of simulation. At 5000rpm conditions, the transition point was at the 10th hour of operation. This primary investigation on the relationship between the piston ring wear and the oil consumption showed that the piston ring wear is indeed an important factor in the oil consumption, which was modeled using the oil vaporization and reverse oil flow.

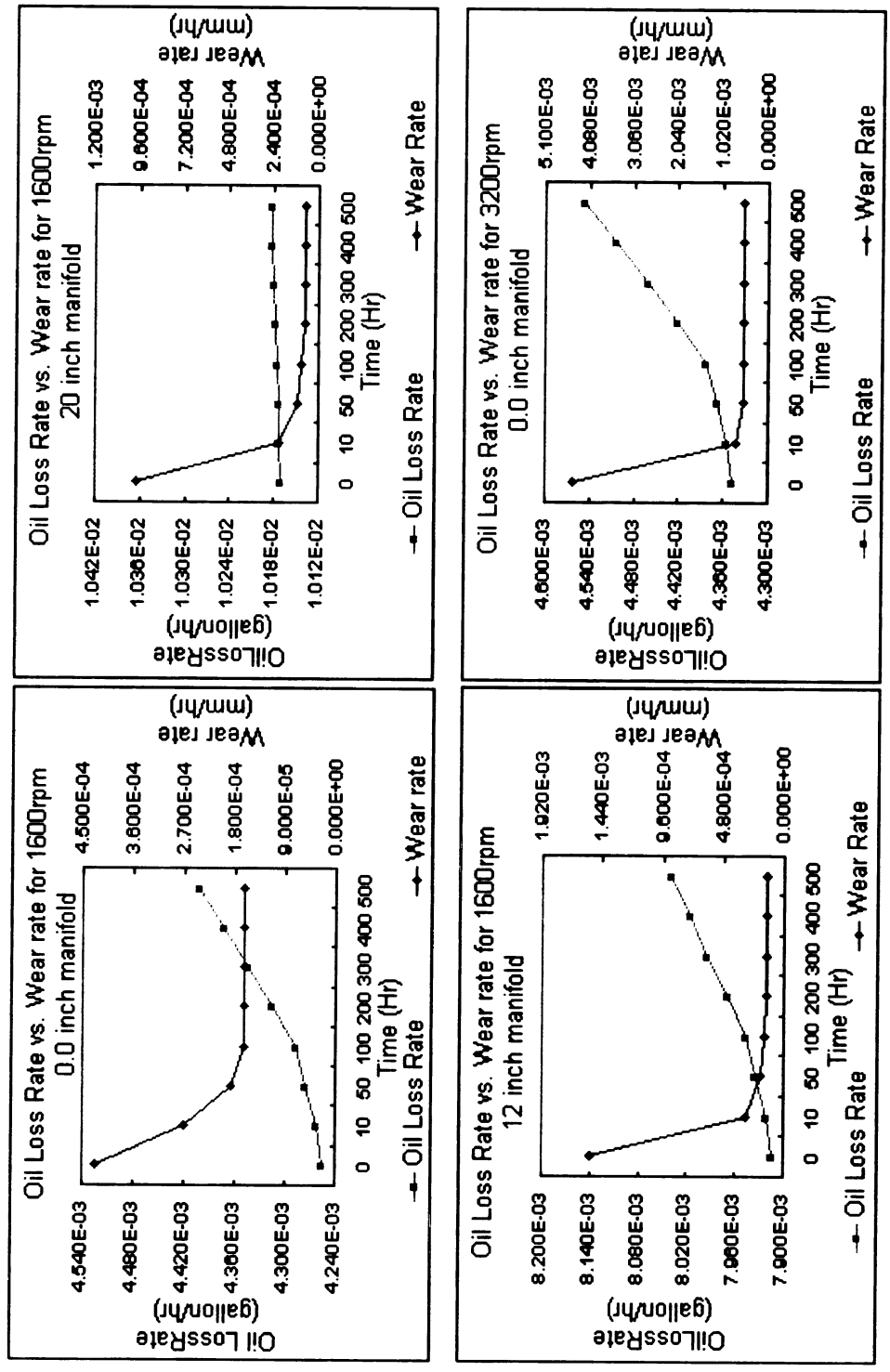

FIGURE 5.44 Oil Loss vs. Wear Rate (I)

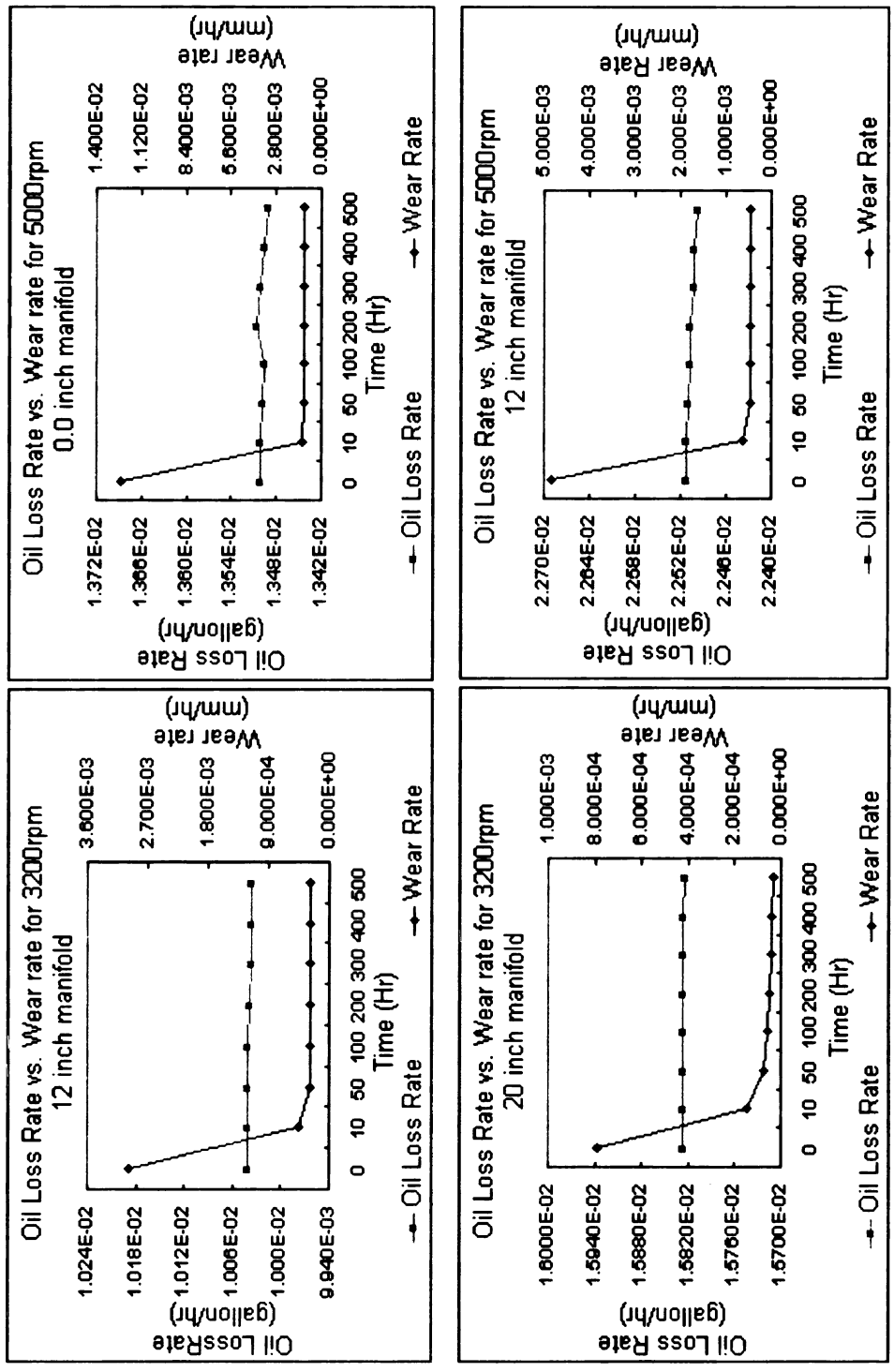

FIGURE 5.45 Oil Loss vs. Wear Rate (II)

Chapter 6 SUMMARY

6.1 Conclusions

In this work, models of piston ring wear and oil consumption were formulated and implemented in a computer model called the CASE system. With the CASE system, the computational design and analysis for a specific engine cylinder kit geometry could be performed. During the analysis presented here, source data from GESIM was developed for a 4.6L, V8 Ford engine and used as input to the CASE system; WEAR and OILCONSUME are the two subroutines, which were developed to be implemented in the CASE system.

In addition to the wear and the oil consumption analyses, the oil film formation, the blow-by and the gas back flow through upper ring gap were also studied in this thesis since they are also important factors in the analysis of an engine performance.

The engine oil consumption model, which included oil vaporization and reverse oil flow mechanisms, did not have significant change over 500 hours of simulation. Practically, the oil consumption would be expected to increase as the age of an engine increases. A significant increase in oil consumption was not observed in this study. This may be due to the fact that not all oil loss mechanisms were included in the simulation. Those oil loss mechanisms not included in this study are oil throw-off, oil carrying through blow-by, valve stem leakage and so on. These mechanisms are more difficult models in a realistic manner, but it will be necessary to include them into the oil

consumption model. Including these mechanisms into the oil consumption model should give a more complete and practical analysis on the oil consumption. For example, the RING generated blow-by results showed significant increase of blow-by over the simulation period. Generally, it is known that the blow-by influences the oil consumption. Therefore, implementing the mechanism of the oil carrying through blow-by would result in the increase of the oil consumption rate over a long time period of engine simulation.

The piston ring wear results of this thesis showed consistency with Chung's mathematical results[1], Barkman's experimental results [2] and Pint's simulation results [3]. High wear rate was observed at the beginning of the simulation and declined exponentially to a steady state value over the simulation period. In addition, the wear was observed to affect the region on the piston ring surface where there were high concentrating stress and influence of the ring twist and piston tilt. The piston ring region on the thrust and anti-thrust sides were observed having higher effect than other locations on the piston ring.

This work also predicted the direct impact of the wear on the blow-by. It was observed that the blow-by increased accordingly to the reduction rate of the ring width. The reduction of the piston ring width due to wear contributed to the increase of the inter-ring volume. Because the inter-ring pressure is a function of the inter-ring volume, and the blow-by is evaluated from the inter-ring pressure, the increase of the inter-ring volume over the simulation period had resulted in the increase of the blow-by.

The engine speed and the engine load were significant factors in affecting an engine performance related to the oil consumption, the piston ring wear, the oil film

formation, the gas back flow and the gas blow-by. It was found in this thesis that both speed and load affect the wear and oil consumption mechanism. This means that low speed did not guarantee low rates of wear and oil consumption, and vice versa. A proper combination of the engine speed and the engine load provides the minimum oil consumption and wear rates. For example, as discussed in Chapter 5, the operating condition of moderate speed(3200rpm) and low engine load (20 inch manifold vacuum) resulted in better oil film formation that kept the piston ring surface at lower wear rate than the condition at 1600rpm. High engine speed (5000rpm) had a high oil film thickness, but did not help in keeping low wear rate.

6.2 Recommendation

Several recommendations were suggested for the future improvement in this research.

1. Reexamination of oil film thickness sensitivity to ring face profile. It was observed in the results that the oil film did not have obvious change even though the piston ring face profile had gone through a drastic change. The input parameter of the piston ring face profile should be increased so that a more complete and detailed description of the piston ring can be evaluated by the RING program.

2. Improvement of the wear model by accommodating more dimension of contacting surfaces. In this thesis, other than the piston ring face and cylinder wall interaction, no other surface interaction are included. The wear related surface-interaction between the piston groove and ring upper surface and bottom surfaces should be studied. Wear on cylinder bore also needs to be included because the hardness and toughness on this surface

is lower (softer) than ring face. In addition, sensitivity studies of surface characteristic on the piston ring with respect to wear should be studied.

3. Improvement of the oil consumption model by accommodating other oil loss mechanisms such as blow-by, oil throw-off, oil burning on the cylinder wall and piston, and valve stem leakage.

4. Obtaining more accurate values for chemical data of engine oil species. Chemical data such as binary diffusion coefficient of two phases of oil vapor and combustion gas need to be obtained so that the oil evaporation model can be modeled more accurately.

BIBLIOGRAPHY

1 Chung, Y. "Development and Analysis of A Fire Ring Wear Model for A Piston Engine". Ph.D. dissertation, Michigan State University, 1992

2 Barkman, D.A. "An Evaluation of The Parameters Involved in Developing A Radiotracer Based Wear Diagnostics System", M.S. thesis, Michigan State University, 1992

3 Pint, S., Schock, H.J., "Design and Development of a Software Module for Analysis of 3-D Piston Ring Wear." SAE Paper 2000-01-0920

4 Ejakov, Mikhail A. "Ring Pack Behavior and Oil Consumption Modeling in IC Engines". PHD dissertation, Michigan State University, 1998

5 Inoue, T., Maeda Y., Takeda M., Nakada M., "Study of Transient Oil Consumption of Automotive Engine". Toyota Motor Corp. 1989

6 Min, B.S., Kim, J.S., Oh, D.Y., Choi, J.K, Jin, J.H., "Dynamic Characteristics of Oil Consumption Relationship Between the Instantaneous Oil Consumption and the Location of Piston Ring Gap". SAE Paper 982442, 1998.

7 Tian, T., Wong, V., Heywood, J.B., "A Piston Ring-Pack Film Thickness and Friction Model for Multigrade Oils and Rough Surfaces." SAE Paper 962032, 1996

8 Wong, V., Audette III W.A., "A Model for Estimating Oil Vaporization from the Cylinder Liner as a Contributing Mechanism to Engine Oil Consumption." SAE Paper 1999-01-1520, 1999

9 Heywood, J.B., "Internal Combustion Engine Fundamentals,"McGraw-Hill, Inc., 1988

10 Nakashima K., Ishihara S., "Influence of Piston Ring Gaps on Lubricating Oil Flow into the Combustion Chamber." SAE Paper 92546, 1992

11 Wilhoit, R.C., Zwolinski, B.J. "Handbook of Vapor Pressures and Heats of Vaporization of Hydrocarbons and Related Compounds." Texas A&M University, 1971.

12 White, Frank M., "Fluid Mechanics".McGraw-Hill, New York, 4th ed., 1999

13 Wong, V., Audette III W.A., "Oil Transport Along the Engine Cylinder Liner Coupling Vaporization and Film-Thickness Analysis." Massachusetts Institute of Technology, 2000

14 Munson, Young, Okiishi, "Fundamentals of Fluid Mechanics." 3rd Ed, John Wiley Sons, Inc. New York, 1998